Opposed regulation of type I IFN-induced STAT3 and ISGF3 transcriptional activities by histone deacetylases (HDACS) 1 and 2

Laura Icardi,*,† Sam Lievens,*,† Raffaele Mori,*,† Julie Piessevaux,*,† Lode De Cauwer,*,† Karolien De Bosscher,*,† and Jan Tavernier*,†,[1]

*Department of Medical Protein Research, Vlaams Instituut voor Biotechnologie, Ghent, Belgium; and †Department of Biochemistry, Faculty of Medicine and Health Sciences, Ghent University, Belgium

ABSTRACT **The antiviral and antiproliferative responses mediated by type I interferons (IFNs) depend on JAK/STAT signaling and ISGF3 (STAT1:STAT2:IRF9)-dependent transcription. In addition, type I IFNs stimulate STAT3 activation in many cell types, an event generally associated with cell cycle progression, survival, and proliferation. To gather more insight into this functionally contradictive phenomenon, we studied the regulation of STAT3 transcriptional activity upon type I IFN treatment. We show that IFNα2 stimulation strongly induces STAT3 phosphorylation, nuclear translocation, and promoter binding, yet the activation of transcription of a STAT3-dependent reporter and endogenous genes, such as *SOCS3* and *c-FOS*, is impaired. Simultaneous treatment with IFNα2 and trichostatin A, as well as combined HDAC1/HDAC2 silencing, restores STAT3-dependent reporter gene and endogenous gene expression, strongly suggesting that HDAC1 and HDAC2 are directly involved in repressing IFNα2-activated STAT3. Of note, single silencing of only one of the two HDACs does not lead to enhanced STAT3 activity, supporting a functional redundancy between these two enzymes. In sharp contrast, HDAC1 and HDAC2 activities are required for ISGF3-dependent gene expression. We conclude that HDAC1 and HDAC2 differentially modulate STAT activity in response to IFNα2: while they are required for the induction of ISGF3-responsive genes, they impair the transcription of STAT3-dependent genes.—Icardi, L., Lievens, S., Mori, R., Piessevaux, J., De Cauwer, L., De Bosscher, K., Tavernier, J. Opposed regulation of type I IFN-induced STAT3 and ISGF3 transcriptional activities by histone deacetylases (HDACS) 1 and 2. *FASEB J.* 26, 240–249 (2012). www.fasebj.org**

Key Words: interferon signaling · trichostatin A · TSA · interferon-stimulated genes

The type I interferon (IFN) family consists of a set of related cytokines, the IFNαs, IFNβs, and IFNωs, that are widely studied for their antiviral (1), antiproliferative, and immunomodulatory properties (2). IFNs elicit these activities through the activation of the IFNα receptor (IFNAR) complex, composed of the IFNAR1 and IFNAR2 chains. Both receptor subunits are devoid of any enzymatic activity but are associated with the Janus kinases (JAKs), TYK2 and JAK1, respectively. The prototypical targets of these tyrosine kinases are members of the signal transducers and activators of transcription (STATs) family, and activation of STAT1 and STAT2 has been studied in great molecular detail. Upon phosphorylation, STAT1 associates with STAT2 and IRF9, leading to the formation of the interferon-stimulated gene factor 3 (ISGF3) complex. ISGF3 acts as transcription factor and binds to the interferon-stimulated responsive element (ISRE), promoting the transcription of the interferon-stimulated genes (ISGs) (3). Additional studies have revealed that type I IFNs can activate all seven STAT family members, leading to the formation of different homodimers and heterodimers, as well as complexes with other transcription factors. These different patterns of STAT activation allow type I IFNs to orchestrate complex and specific biological responses in diverse cell types and under different physiological or pathological conditions (4).

Of particular interest are the mechanisms controlling the activity of STAT3, since its persistent activation has been observed in a high number of human cancers (5). As reviewed by van Boxel-Dezaire *et al.* (4), IFNα stimulation was reported to trigger STAT3 activation in various cell types. In response to cytokine stimulation, STAT3 becomes rapidly phosphorylated at Tyr705 by the JAKs. This phosphorylation is required for STAT3 dimerization, nuclear translocation, DNA binding, and transcriptional activity (6). In addition, phosphorylation of a single serine residue (Ser727) in the transcriptional activation domain is required for maximal transcriptional activation (7). Recent studies showed that,

[1] Correspondence: Department of Medical Protein Research, Vlaams Instituut voor Biotechnologie, B-9000 Ghent, Belgium. E-mail: jan.tavernier@vib-ugent.be

doi: 10.1096/fj.11-191122

This article includes supplemental data. Please visit *http://www.fasebj.org* to obtain this information.

0892-6638/12/0026-0240 © FASEB

in addition to phosphorylation, inducible lysine acetylation also has a central role in promoting the transcriptional activity of STAT3 (8–9). Of note, different lysines of STAT3 have been reported to be acetylated, and different patterns of acetylation have a different effect on its transcriptional activity. STAT3 acetylation is efficiently reverted by the histone deacetylases HDAC1, HDAC2, and HDAC3 (9–11), which directly associate with STAT3 and contribute to its negative regulation. Activated STAT3 stimulates the transcription of several genes involved in cell cycle progression, such as *c-MYC*, *PIM1*, and *CYCLIN D1*, and also up-regulates antiapoptotic genes such as *BCL-2* and *BCL-X* (12). In addition, for its ability to transform normal fibroblast cells and cause tumors in nude mice, STAT3 has been classified as an oncogene (13). These effects are in sharp contrast with the proapoptotic and antiproliferative effects triggered by IFNs, which provide the rationale for their use in cancer therapy. To achieve a more detailed insight into the regulation of STAT3 in the IFNα signaling pathway, we investigate here its transcriptional activity, downstream of its activation by phosphorylation.

We report that, upon IFNα2 treatment, the transcriptional activity of STAT3 is impaired, although its phosphorylation, nuclear translocation, and promoter binding are strongly induced and comparable to a positive control [leukemia-induced factor (LIF) treatment]. Interestingly, we find that the activities of HDAC1 and HDAC2, but not HDAC3, are directly involved in the negative regulation of STAT3 transcriptional activity. Indeed, interfering with HDAC1 and HDAC2 enzymatic functions, through trichostatin A treatment or combined siRNA-mediated silencing, restores the activation of both a STAT3-dependent reporter gene and STAT3-driven endogenous gene transcription. Of particular interest, recent observations showed that the activity of HDAC1 is crucial for the IFN-stimulated innate antiviral immunity, which relies on the activation of ISGF3-regulated genes (14). In line herewith, our results show that interfering with the function of both HDAC1 and HDAC2 impairs the activation of ISGF3-regulated genes and simultaneously relieves a "frozen" pretranscriptional state of STAT3. In summary, our study indicates that HDAC1 and HDAC2 play a key role in the modulation of the IFNα response, exerting opposing regulation on ISGF3- and STAT3-dependent signaling. In addition, it unveils a hitherto unknown late-stage mechanism to suppress STAT3 transcriptional activity.

MATERIALS AND METHODS

Plasmids, cytokines, and drug treatments

The generation of the pXP2d2-rPAP1-luciferase reporter, originating from the rat pancreatitis-associated protein 1 (rPAP1) promoter was described previously (15). The plasmid pCAGGS-HA-STAT3Y705F (dominant negative) was a gift from Dr. Toshio Hirano (Laboratory of Developmental Immunology, Osaka University, Osaka, Japan). The plasmid pMET7-Etag-hSTAT3 was constructed using the primer pair 5′-GCGGCGGCCGCAGCCCAATGGAATCAGCTACAG-3′ and 5′-CGCCTCGAGTCACATGGGGGAGGTAGCGCA-3′ to clone STAT3 into the pMET7 vector. The generation of Flp-In T-Rex HEK293 cells stably expressing the pXP2d2-rPAP1-luciferase reporter is described elsewhere (16). Recombinant human IFNα2 (PBL Interferon Source, Piscataway, NJ, USA) and recombinant human LIF (Millipore, Billerica, MA, USA) were used at 10 ng/ml unless specified otherwise. Trichostatin A (Sigma Aldrich, St. Louis, MO, USA) was used at 100 ng/ml and was added to the cell medium together with the cytokine stimulation.

Plasmid transfection protocols and luciferase assay

For plasmid transfection experiments, HEK293T cells were transfected overnight with 1 μg of plasmid pCAGGS-HA-STAT3Y705F, using a standard calcium phosphate precipitation procedure (17). The pMet7 empty vector construct was used to normalize for the amount of transfected DNA. For the acetylation assay, HEK293T cells were plated in 10-cm Petri dishes and transfected overnight with 5 μg of plasmid pMET7-Etag-hSTAT3. For the luciferase assays, cells were transfected with the luciferase reporter vectors with the molar ratio (1:5) of reporter vector to expression vector. The next day, cells were washed with PBS, trypsinized, transferred to a 96-well plate, and left untreated or stimulated with the indicated amount of IFNα2 or LIF for 24 h. Luciferase activity from triplicate samples was measured by chemiluminescence with a TopCount luminometer (Canberra-Packard, Waverley, UK) and expressed as fold induction (stimulated/nonstimulated).

Lysate preparation, Western blot analysis, and immunoprecipitation

At 48 h after transfection, cells were cultured for 4 h without FCS, stimulated, and lysed with 200 μl of modified RIPA lysis buffer (200 mM NaCl; 50 mM Tris-HCl, pH 8; 0.05% SDS; 2 mM EDTA; 1% Nonidet P-40; 0.5% sodium deoxycholate; 1 mM Na_3VO_4; 1 mM NaF; and Complete Protease Inhibitor Cocktail; Roche Applied Science, Penzberg, Germany). For the acetylation assay, cells were transfected with Etag-hSTAT3, cultured 4 h without FCS, stimulated, and lysed with 1 ml of modified RIPA lysis buffer plus 1 μM trichostatin A (TSA). Lysates were incubated with an anti-acetyl lysine antibody (Cell Signaling Technology, Danvers, MA, USA) overnight at 4°C. Immune complexes were precipitated by adding 30 μl of protein A-Sepharose beads (50% slurry) and rotated for 2 h at 4°C. Beads were washed 3 times with modified RIPA buffer, incubated with 10 μl of 5× SDS loading buffer, and boiled at 98°C for 10 min. Lysates were loaded on a 10% SDS-polyacrylamide gel and transferred to a nitrocellulose membrane (Amersham, Dubendorf, Switzerland). The following antibodies were used: rabbit polyclonal antibodies against endogenous STAT3 and phosphorylated Y_{705}STAT3 and mouse monoclonal antibodies against HDAC1, HDAC2, HDAC3, and LAMIN A/C were purchased from Cell Signaling Technology; expression levels of HA-tagged STAT3Y705F plasmid were revealed using an anti-HA-tag monoclonal antibody from Boehringer Mannheim (Mannheim, Germany); anti-ACTIN mouse monoclonal antibody was purchased from Sigma Aldrich; mouse monoclonal antibody against GAPDH was purchased from Abcam (Cambridge, UK); either goat anti-mouse Dylight 800 or anti-rabbit Dylight 680 (Pierce, Rockford, IL, USA) was used as secondary Ab. Targeted proteins on the blots were visualized using

the Odyssey infrared imaging system (LI-COR Biosciences, Lincoln, NE, USA).

Nuclear extract preparation and STAT3-DNA binding assay

Nuclear extracts were prepared as described previously (18), yet slightly modified. In brief, cells were washed with PBS and resuspended in 400 μl ice-cold hypotonic buffer (10 mM Tris-HCl, pH 7.8; 5 mM $MgCl_2$; 10 mM KCl; 0.1 mM EDTA; 300 mM sucrose; 5 mM β-glycerophosphate; 0.5 mM DTT; and Complete Protease Inhibitor Cocktail). The cell suspension was briefly vortexed and allowed to swell for 15 min. Cells were then lysed by adding a final concentration of 0.5% Nonidet P-40, vortexing and incubating 10 min on ice. Afterward, nuclei were precipitated (1 min at 2000 rpm), and supernatant was removed. Isolated nuclei were washed 3 times in hypotonic buffer (after each wash, precipitated at 2000 rpm for 1 min). The nuclear pellet was lysed in 50 μl hypertonic buffer (20 mM Tris-Cl, pH 7.8, 5 mM $MgCl_2$; 320 mM KCl; 0.2 mM EDTA; 25% glycerol; 0.5 mM DTT; 5 mM β-glycerophosphate; and Complete Protease Inhibitor Cocktail) and was incubated on ice for 30 min. Nuclear debris was removed through centrifugation at 13,000 rpm for 10 min. For the STAT3-DNA binding assay, the TransAM STAT3 kit (Active Motif, Carlsbad, CA, USA) was used following manufacturer's instructions.

Chromatin immunoprecipitation (ChIP) assays

Cells were cultured for 4 h in serum-free medium and stimulated with IFNα2 or LIF for 30 min, followed by fixation with 1% formaldehyde at room temperature for 10 min. Fixation was quenched by the addition of 2 M glycine at the final concentration of 10%, then cells were washed twice with PBS plus 0.5 mM EDTA. Cells were collected and sonicated in PBS plus 0.5 mM EDTA to shear the chromatin DNA to fragments of 500-1000 bp. The supernatant was clarified by centrifugation and 1/10 of the sonicated chromatin was saved as input. The remaining chromatin solution was incubated with rabbit polyclonal anti-STAT3 (Cell Signaling Technology) and rabbit polyclonal anti-STAT3 (Santa Cruz Biotechnology, Santa Cruz, CA, USA) antibodies or normal rabbit immunoglobulin G (Santa Cruz Biotechnology) at 4°C overnight. Antibody-protein-DNA complexes were incubated with Protein A Sepharose 4 Fast Flow (Amersham), and immunoprecipitates were washed once with RIPA buffer (10 mM Tris-HCl, pH 8; 150 mM NaCl; 0.1% SDS; 1% Nonidet P-40; 0.1% sodium deoxycholate; and Complete Protease Inhibitor Cocktail), twice with RIPA-500 buffer (10 mM Tris-HCl, pH 8; 500 mM NaCl; 0.1% SDS; 1% Nonidet P-40; 0.1% sodium deoxycholate; and Complete Protease Inhibitor Cocktail), once with LiCl buffer (10 mM Tris-HCl, pH 8; 250 mM LiCl; 0.5% Nonidet P-40; 0.5% sodium deoxycholate; 1 mM EDTA; and Complete Protease Inhibitor Cocktail), and one last time with TBS buffer (20 mM Tris-HCl, pH 7.6; and 137 mM NaCl). Bound proteins were eluted from the beads in elution buffer (1% SDS and 0.1 M $NaHCO_3$) by incubation at room temperature for 30 min while shaking. Cross-linking was reverted by incubation at 65°C overnight. All samples were treated with 50 ng/μl of RNase A and 100 ng/μl of Proteinase K. DNA fragments were purified using the QIAquick PCR purification kit (Qiagen, Venlo, Netherlands) and subjected to quantitative PCR using SYBR Green Master (Roche Applied Science) with the specific primer set for *c-FOS*: 5-GCAGCCCGCGAGCAGTT-3 (forward), 5-GCCTTGGCGCGTGTCCTAATC-3 (reverse). For *SOCS3*, the Universal ProbeLibrary Assay (Roche Applied Science) was used with primers 5-AAAAGGGGAAGGGGAACC-3 (forward) and 5-GGAGAGCGGGCAGTTCTA-3 (reverse) in combination with probe 85. The results were analyzed using the $\Delta\Delta C_T$ method. The fold change of STAT3 promoter occupancy was calculated by normalizing the relative amount to the input and comparing with untreated cells.

siRNA transfection

Renilla luciferase (*RL*), *HDAC1*, *HDAC2*, and *HDAC3* siRNA On-Target Plus SMARTpools were purchased from Thermo Scientific (Dharmacon RNAi Technology, Lafayette, CO, USA) and transfection (siRNA final concentration 50 nM) was performed following the manufacturer's instructions. Western blot analysis to verify silencing efficiency and cytokine stimulation for the luciferase assays were performed at 72 h after transfection.

Quantitative RT-PCR (qRT-PCR)

Cell lysates were homogenized with the QiaShredder Column (Qiagen), and total cellular RNA was extracted with the RNeasy Mini kit (Qiagen) following manufacturer's instructions. Equal amounts of RNA (0.5 μg) were used for reverse transcription using the Primescript RT Reagent kit (Takara Bio, Shiga, Japan), following the manufacturer's instructions. A 1:20 dilution of the cDNA products was amplified in quantitative PCR following the Universal ProbeLibrary System (Roche Applied Science) guidelines and processed in a LightCycler 480 Real-Time PCR System thermocycler (Roche Applied Science), and the results were analyzed using the $\Delta\Delta C_T$ method. The primers and the probes used in the assays were selected with the online tool Universal ProbeLibrary Assay Design Center (Roche Applied Science) and were as follows: human *GAPDH* 5-AGCCACATCGCTCAGACAC-3 (forward), 5-GCCCAATACGACCAAATCC-3 (reverse) in combination with probe 60; human *SOCS3* 5-CTTCGACTGCGTGCTCAA-3 (forward), 5-GTAGGTGGCGAGGGGAAG-3 (reverse) in combination with probe 1; human c-*FOS* 5-CTACCACTCACCCGCAGACT-3 (forward), 5-AGGTCCGTGCAGAAGTCCT-3 (reverse) in combination with probe 67; human *EGR1* 5-AGCCCTACGAGCACCTGAC-3 (forward), 5-GGTTTGGCTGGGGTAACTG-3 (reverse) in combination with probe #22, human *ISG15* 5-GCGAACTCATCTTTGCCAGT-3 (forward), 5-AGCATCTTCACCGTCAGGTC-3 (reverse) in combination with probe 76; human *ISG54* 5-TGGTGGCAGAAGAGGAAGAT-3 (forward), 5-GTAGGCTGCTCTCCAAGGAA-3 (reverse) in combination with probe 27; human *2′5′OAS* 5-GACGGATGTTAGCCTGCTG-3 (forward), 5-TGGGGATTTGGTTTGGTG-3 (reverse) in combination with probe 43. The fold change of mRNA expression was calculated by normalizing the relative amount to the internal control *GAPDH* and comparing with untreated cells or cells treated with *Renilla luciferase* (*RL*) siRNA.

Immunofluorescence analysis and confocal microscopy

Cells were seeded on coverslips and grown in serum-free medium for 16 h. Fixation, permeabilization, and staining were performed as described previously (19). STAT3 was visualized with a 1:1600 dilution of the anti-STAT3 antibody, followed by probing with a 1:300 dilution of Alexa Fluor 488-conjugated goat anti-mouse IgG. Staining with 4,6-diamidino-2-phenylindole (DAPI) was used to stain the cell nuclei. A motorized inverted IX81 FluoView FV1000 laser scanning confocal microscope (Olympus, Tokyo, Japan) was used to record high-resolution images.

RESULTS

Uncoupling of STAT3 phosphorylation and STAT3-responsive gene induction in type I IFN signaling

Type I IFNs were reported to induce STAT3 phosphorylation in various cell types (4). Since phosphorylation of STAT3 on Tyr705 has been widely used as a marker for its activity as a transcription factor, we first analyzed STAT3 phosphorylation and STAT3 transcriptional activity on IFNα2 treatment. Therefore, HEK293T cells were stimulated with increasing amounts of IFNα2, and the total lysates were immunoblotted to detect endogenous STAT3 Tyr705 phosphorylation (**Fig. 1*A***). As expected, IFNα2 stimulation strongly induced STAT3 phosphorylation, in a dose-dependent manner. Next, we compared the kinetics of STAT3 activation on treatment with IFNα2 and LIF. LIF is a member of the IL-6 cytokine subfamily known to signal mainly through the activation of STAT3 (20) and is here used as a positive control for STAT3 activity. Figure 1*B* shows that not only LIF but also IFNα2, albeit slightly weaker, could induce a marked phosphorylation of STAT3. IFNα2 induced a strong STAT3 phosphorylation 30 min after treatment, which decreased slowly with time. Of note, LIF treatment led to a prolonged phosphorylation of STAT3, still evident 24 h after stimulation. Besides phosphorylation, the transcriptional activity of STAT3 is additionally regulated by the acetylation of multiple lysine residues (8–9, 21). For this reason, we analyzed the levels of STAT3 acetylation after IFNα2 and LIF treatment. Figure 1*C* shows that both cytokines

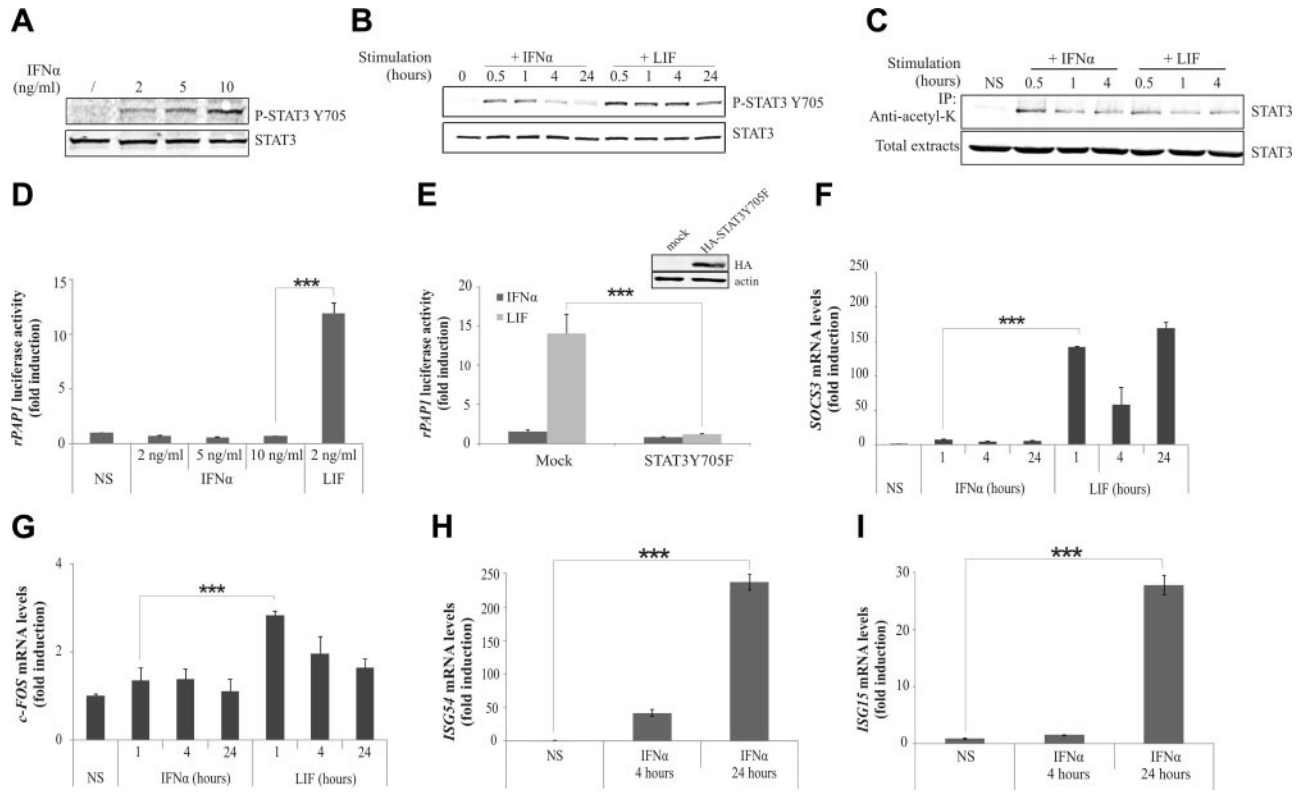

Figure 1. Uncoupling of STAT3 phosphorylation/acetylation and STAT3-mediated gene induction in type I IFN signaling. *A*) Dose-dependent phosphorylation of STAT3 upon IFNα2 stimulation. HEK293T cells were cultured for 4 h in DMEM without FCS and then stimulated with the indicated amounts of IFNα2 for 20 min. Total cell extracts were blotted with anti-phospho STAT3 (Tyr705) and anti-STAT3 antibody. *B*) Kinetics of STAT3 phosphorylation on IFNα2 and LIF treatment. HEK293T cells were cultured for 4 h in DMEM without FCS and then stimulated with IFNα2 or LIF (both 10 ng/ml) for the indicated time periods. Total cell extracts were blotted with anti-phospho STAT3 (Tyr705) and anti-STAT3 antibody. *C*) Kinetics of STAT3 acetylation on IFNα2 and LIF treatment. HEK293T cells were transfected with pMET7-Etag-hSTAT3 for 48 h, cultured for 4 h in DMEM without FCS, and then stimulated with IFNα2 or LIF (both 10 ng/ml) for the indicated time periods. Acetylated lysines were immunoprecipitated with an anti-acetyl lysine antibody, and acetylated STAT3 was revealed with an anti-STAT3 antibody. Total lysates were collected before immunoprecipitation and blotted with anti-STAT3 antibody. *D*, *E*) Impaired STAT3 transcriptional activity on IFNα2 treatment. HEK293T cells were transiently transfected with the pXP2d2-rPAP1-luciferase reporter alone (*D*) or together with the pCAGGS-HA-STAT3Y705F (*E*) and left nonstimulated (NS) or stimulated for 24 h with the indicated amount of IFNα2 or LIF (or 10 ng/ml if not specified). Luciferase readout is expressed as a ratio between stimulated and unstimulated values. $***P < 0.001$; *t* test. *F–I*) qRT-PCR analysis representing the relative mRNA levels of *SOCS3* (*F*), c-*FOS* (*G*), *ISG54* (*H*), and *ISG15* (*I*). HEK293T cells were cultured 4 h in DMEM without FCS and then left nonstimulated or stimulated with IFNα2 or LIF (both 10 ng/ml) for the indicated time points. Graphs represent the mRNA levels relative to the nonstimulated samples. All results are representative of 3 independent experiments. Error bars indicate SD from triplicates. $***P < 0.001$; 1-way ANOVA with Bonferroni test.

induced STAT3 acetylation at comparable levels, with a peak at 30 min after stimulation. We further investigated the transcriptional activity of STAT3 in type I IFN signaling by measuring the activation of a STAT3-dependent reporter, consisting of the luciferase reporter gene under control of the rPAP1 promoter. HEK293T cells were transiently transfected with the rPAP1 reporter and stimulated with IFNα2 or LIF. Interestingly, we found that IFNα2 stimulation completely failed to activate the rPAP1 reporter (Fig. 1*D*), in contrast to LIF treatment. To demonstrate the specificity of the rPAP1 promoter for activated STAT3, the cells were cotransfected with a dominant negative form of STAT3 (STAT3Y705F), where the tyrosine 705 is mutated to phenylalanine. Figure 1*E* shows that the presence of a dominant negative form of STAT3 completely abrogated the activation of the reporter. Next, we investigated whether, upon IFNα2 treatment, phosphorylated STAT3 would induce the transcription of the endogenous genes *SOCS3* and *c-FOS*, two known target genes of activated STAT3. HEK293T cells were stimulated for different time periods with either IFNα2 or LIF, and transcription of *SOCS3* and *c-FOS* genes was measured by qRT-PCR. In agreement with the reporter-based assay and again in strong contrast with LIF treatment, IFNα2 treatment failed to induce *SOCS3* and *c-FOS* gene transcription (Fig. 1*F, G*). As expected, IFNα2 treatment strongly induced the transcription of the ISGF3-responsive genes *ISG54* and *ISG15* (Fig. 1*H, I*). Taken together, these results show that IFNα2 treatment stimulates STAT3 phosphorylation and acetylation but, surprisingly, STAT3 transcriptional activity is impaired. We conclude that STAT3 activation (through phosphorylation/acetylation) and STAT3 transcriptional activity are different processes that can be uncoupled.

IFNα-induces STAT3 nuclear translocation and DNA binding

The inhibition of STAT3 transcriptional activity observed after IFNα stimulation can be due to an impaired nuclear translocation or DNA binding. To evaluate these possibilities, we prepared nuclear, cytoplasmic, and total extracts after IFNα2 or LIF stimulation of HEK293T cells and checked for the presence of phosphorylated STAT3. As shown in **Fig. 2*A***, both IFNα2 and LIF stimulation led to a comparable partial accumulation of phospho-STAT3 in the nucleus. Next, the ability of STAT3 to bind DNA after IFNα2 treatment was assayed. The nuclear extracts of IFNα2- or LIF-stimulated cells were incubated with immobilized oligonucleotides containing a generic STAT-consensus binding site (5′-TTCCCGGAA-3′), and bound endogenous STAT3 was detected using a specific anti-STAT3 antibody. As shown in Fig. 2*B*, both cytokines stimulated STAT3 binding to the STAT-consensus DNA sequence. Taken together, these results indicate that the impairment of STAT3-dependent gene transcription is not due to lack of nuclear translocation or DNA-binding of the transcription factor. We next asked whether IFNα2 stimulation would lead to the recruitment of STAT3 to the endogenous promoters of *SOCS3* and *c-FOS* genes. HEK293T cells were stimulated with either IFNα2 or LIF, and the occupancy of STAT3 on the promoters was investigated by ChIP assays. Figure 2*C* shows that IFNα2 strongly induced the recruitment of STAT3 at the *c-FOS* promoter, to a similar extent as LIF treatment. IFNα2

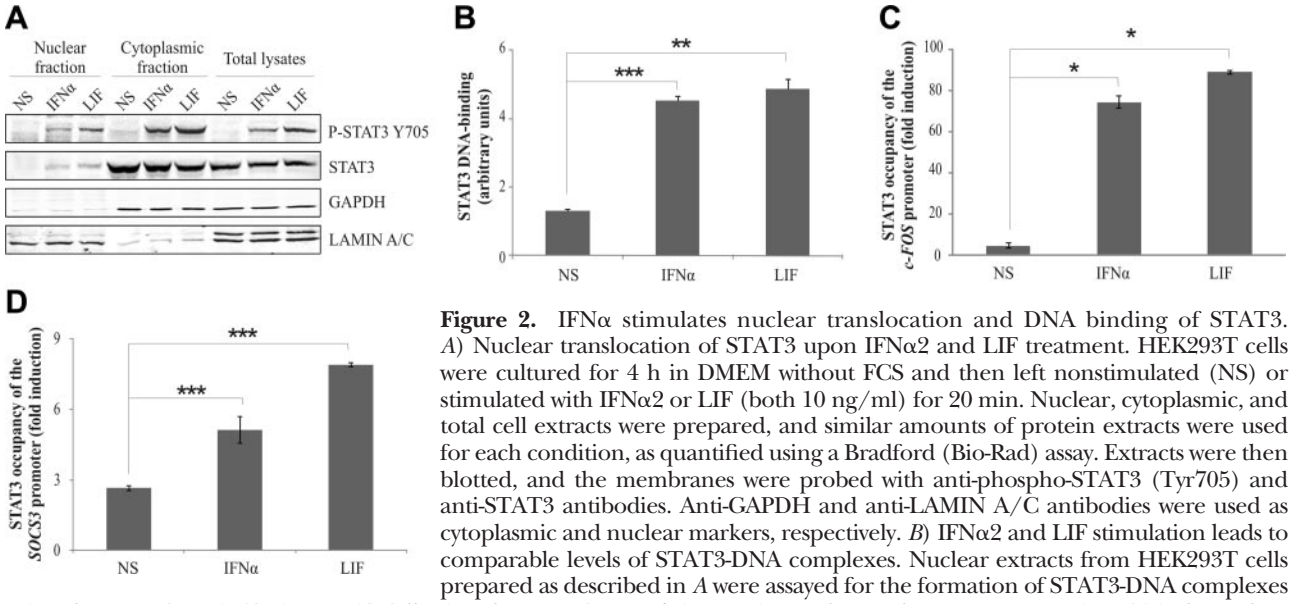

Figure 2. IFNα stimulates nuclear translocation and DNA binding of STAT3. *A*) Nuclear translocation of STAT3 upon IFNα2 and LIF treatment. HEK293T cells were cultured for 4 h in DMEM without FCS and then left nonstimulated (NS) or stimulated with IFNα2 or LIF (both 10 ng/ml) for 20 min. Nuclear, cytoplasmic, and total cell extracts were prepared, and similar amounts of protein extracts were used for each condition, as quantified using a Bradford (Bio-Rad) assay. Extracts were then blotted, and the membranes were probed with anti-phospho-STAT3 (Tyr705) and anti-STAT3 antibodies. Anti-GAPDH and anti-LAMIN A/C antibodies were used as cytoplasmic and nuclear markers, respectively. *B*) IFNα2 and LIF stimulation leads to comparable levels of STAT3-DNA complexes. Nuclear extracts from HEK293T cells prepared as described in *A* were assayed for the formation of STAT3-DNA complexes using the TransAm Kit (Active Motif) following the manufacturer's instructions. The results are representative of 2 independent experiments. $^{**}P < 0.01$, $^{***}P < 0.001$; *t* test. *C, D*) STAT3 binds to the endogenous *c-FOS* and *SOCS3* promoters. ChIP assays were performed to examine the occupancy of STAT3 on the *c-FOS* (*C*) and *SOCS3* (*D*) promoters, as described in Materials and Methods. Immunoprecipitated DNA from nonstimulated or IFNα2 or LIF stimulated (both 10 ng/ml, 30 min) HEK293T cells was subjected to qRT-PCR using primers specific for the two promoters. Graphs represent STAT3 occupancy levels relative to NS sample. Results are representative of 3 independent experiments. Error bars indicate SD from triplicates. $^{*}P < 0.05$, $^{***}P < 0.001$; 1-way ANOVA with Bonferroni test.

stimulation also induced the recruitment of STAT3 at the *SOCS3* promoter, as shown in Fig. 2*D*, although to a lesser extent than LIF treatment. In summary, these data show that IFNα2 stimulates the nuclear translocation of phospho-STAT3 and its recruitment to the STAT3-responsive promoters, *c-FOS* and *SOCS3*, without activating their transcription.

Simultaneous treatment with IFNα and TSA leads to the restoration of IFN-dependent STAT3 transcriptional activity

The transcriptional activity of STAT3 has been shown to be positively regulated by the acetylation of multiple lysine residues (8–9, 22). As a consequence, the activity of STAT3 can be downmodulated by the interaction with different HDACs (9–11). In this context, we asked whether deacetylation could explain the hampered transcriptional activity of STAT3. Therefore, Flp-In T-Rex HEK293 cells stably expressing the rPAP1-luciferase reporter were simultaneously stimulated with IFNα2 and with the potent HDACs inhibitor TSA, and then compared to the samples stimulated with either IFNα2 or TSA. Clearly, cotreatment of the cells with both TSA and IFNα2 restored the transcriptional activity of STAT3, as shown by the activation of the rPAP1 reporter (**Fig. 3*A***). Of note, Fig. 3*B* shows that, although cotreatment with IFNα2 and TSA restored STAT3-dependent transcription, it did not alter the phosphorylation pattern of STAT3, suggesting the presence of a regulatory mechanism acting downstream of the phosphorylation event. In agreement with the reporter assay, the combined stimulation with TSA and IFNα2 also led to the transcription of the STAT3-stimulated *c-FOS* and *EGR1* genes in the 2fTGH cell line (Fig. 3*C*, *D*), further demonstrating that the activity of the HDACs is directly involved in the repression of STAT3-responsive genes on IFNα2 treatment. Of note, in the same cell line and using the same stimuli, TSA efficiently abrogated the expression of the ISGF3-responsive genes *ISG15* and *ISG54* induced by IFNα2 treatment (Fig. 3*E*, *F*). We next assessed the dynamics of the subcellular localization of endogenous STAT3 by confocal microscopy imaging on 2fTGH cells stimu-

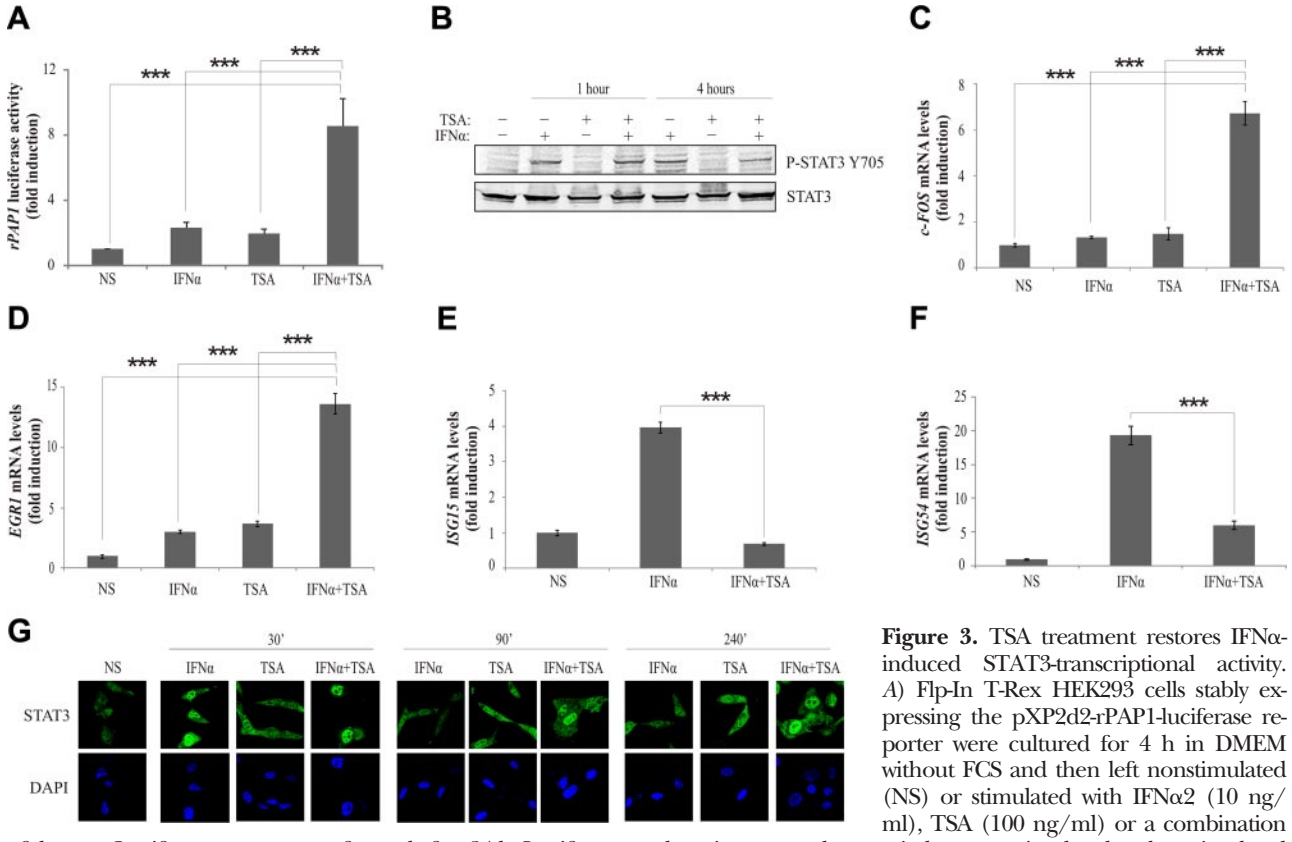

Figure 3. TSA treatment restores IFNα-induced STAT3-transcriptional activity. *A*) Flp-In T-Rex HEK293 cells stably expressing the pXP2d2-rPAP1-luciferase reporter were cultured for 4 h in DMEM without FCS and then left nonstimulated (NS) or stimulated with IFNα2 (10 ng/ml), TSA (100 ng/ml) or a combination of the two. Luciferase assay was performed after 24 h. Luciferase read-out is expressed as a ratio between stimulated and unstimulated values. ***$P < 0.001$; *t* test. *B*) TSA treatment does not influence STAT3 Y705 phosphorylation. HEK293 cells were cultured for 4 h in DMEM without FCS and then left nonstimulated or stimulated with IFNα2 (10 ng/ml), TSA (100 ng/ml), or a combination of the two for the indicated time periods. Total cell extracts were blotted with anti-phospho STAT3 (Tyr705) and anti-STAT3 antibody. *C–F*) qRT-PCR analysis representing the relative mRNA levels of the STAT3-responsive c-*FOS* (*C*) and *EGR1* (*D*) genes and the ISGF3-responsive *ISG15* (*E*) and *ISG54* (*F*) genes. 2fTGH cells were cultured 4 h in DMEM without FCS, then left nonstimulated or stimulated with IFNα2 (10 ng/ml), TSA (100 ng/ml), or a combination of the two for 24 h. Graphs represent mRNA levels relative to NS sample. Results are representative of 3 independent experiments. Error bars indicate SD from triplicates. ***$P < 0.001$; 1-way ANOVA with Bonferroni test. *G*) Accumulation of nuclear STAT3 after combined TSA and IFNα treatment. 2fTGH cells were starved for 16 h. Solvent, TSA (100 ng/ml), and/or IFNα (10 ng/ml) were added for the indicated times. Cells were fixed and stained, and the localization of STAT3 was assessed by confocal analysis. Confocal immunofluorescence of representative cell fields is shown.

lated with IFNα2, TSA, or both (Fig. 3*G* and Supplemental Fig. S1). In solvent-treated cells, STAT3 was evenly distributed over both the cytoplasm and nucleus. IFNα2 treatment for 30 min induced an enhanced nuclear accumulation of STAT3, which then redistributed back to the cytoplasm at later time points. Of note, when cells were simultaneously treated with IFNα2 and TSA, STAT3 showed a prolonged accumulation in the nucleus even after 4 h of stimulation, indicating that the activity of HDACs may affect the nuclear-cytoplasmic distribution of STAT3.

The activity of HDAC1 and HDAC2, but not HDAC3, contributes to the inhibition of STAT3 transcriptional activity on IFNα treatment

The acetylation status of STAT3 is counteracted by its association with HDAC1, HDAC2, and HDAC3 (9–11). The NH_2 terminus of these HDACs contains a motif required for their homooligomerization. In addition, heterooligomers have been reported for HDAC1 with HDAC2 and HDAC3 (22, 23). We asked whether these HDACs could be involved in the IFN-driven inhibition of STAT3 activity. The Flp-In T-Rex HEK293 cells stably expressing the rPAP1-luciferase reporter were first transfected with an irrelevant siRNA (*Renilla luciferase* siRNA) or with siRNAs targeting the HDACs and then stimulated with IFNα2. Since functional redundancy in HDAC activity is possible, the three HDACs were silenced individually or in pair-wise combination (**Fig. 4*A***). Interestingly, the combined silencing of HDAC1 and HDAC2, but not HDAC3, enhanced the IFN-dependent STAT3 transcriptional activity. In agreement with this observation, the transcription of *SOCS3* was also induced by IFNα2 treatment in HEK293T on combined HDAC1/HDAC2 silencing (Fig. 4*B*). Silencing efficiency was evaluated by immunoblotting of the total lysates with specific antibodies against the endogenous HDAC1, HDAC2, and HDAC3 (Fig. 4*C*). Of note, the efficiency of the combined silencing of HDAC1 and HDAC2 was reproducibly inferior compared to the single silencing. This is in line with the previous observation that depletion of either HDAC1 or HDAC2 causes a compensatory up-regulation of HDAC2 and HDAC1, respectively (24). Next, we analyzed the effect of HDAC1/HDAC2 silencing on MCF7 breast cancer cells. Interestingly, in this cell line, IFNα2 stimulation led to the transcription of the STAT3-responsive genes *SOCS3* and *EGR1* (Fig. 4*D*, *E*). Nonetheless, silencing of the two HDACs further raised the levels of their expression. In sharp contrast, interfering with HDAC1 and HDAC2 activities impaired the transcription of the ISGF3-dependent gene *ISG54* (Fig. 4*F*). We next asked whether a combined silencing of HDAC1 and HDAC2 would affect the subcellular localization of STAT3, as observed with TSA treatment (Fig. 3*G* and Supplemental Fig. S1). To this aim, MCF7 cells were transfected with an irrelevant (*Renilla luciferase*) siRNA or a combination of HDAC1 and HDAC2 siRNA. As shown in Fig. 4*G* and Supplemental Fig. S2, IFNα2 treatment of MCF7 cells led to a transient nuclear accumulation of STAT3, peaking at 30 min. Of note, HDAC1/HDAC2 silencing led to a prolonged accumulation of STAT3 in the nucleus, even 4 h after IFNα2 treatment, a time when STAT3 is normally redistributed back to the cytoplasm (RL siRNA panels). In summary, we show that HDACs, and, in particular, HDAC1 and HDAC2, exert opposed regulation on STAT3- and ISGF3-responsive gene transcription: their activity represses STAT3-dependent genes, while, on the other hand, they are necessary for the expression of ISGF3-dependent genes.

DISCUSSION

The activation of STAT3 upon type I IFN stimulation has been documented in a number of different cell types (4), but its role in type I IFN signaling is not fully understood. Whereas STAT3 activation generally promotes cell cycle progression, survival, and proliferation (12), type I IFN stimulation triggers cell apoptosis or growth arrest (25). To better understand this functionally contradictive observation, we investigated the regulation of the transcriptional activity of STAT3 in the IFNα signaling pathway. Here, we show that, on IFNα2 treatment, STAT3 phosphorylation, nuclear translocation, and DNA binding are strongly induced and comparable to LIF treatment (positive control for STAT3 activation). Yet, in contrast with LIF, IFNα2 stimulation fails to activate the transcription of the STAT3-dependent genes *SOCS3* and *c-FOS*, although STAT3 is efficiently recruited at their promoters. Comparing IFNα2 and LIF treatment, we could not detect a significant difference in the degree of STAT3 Tyr705 phosphorylation that would explain the disparity in its transcriptional activity. Beside phosphorylation, other post-translational modifications have been reported to modulate STAT3 activity. Among these, acetylation, exerted by the histone acetyltransferases (HATs) p300 and CBP (26), appears to be a critical determinant in the regulation of STAT3 activity. STAT3 undergoes acetylation on different lysine residues in response to various cytokine stimuli. Acetylation positively regulates STAT3 transcriptional activity, although the precise effect of this modification depends on the acetylated residue. For instance, acetylation of STAT3 on K685 is necessary for dimer stability, a correct nucleocytoplasmic distribution, and DNA binding (9, 26). IFNα has been reported to promote STAT3 acetylation on K685, as well as many cytokines belonging to the IL6 family, such as IL6, LIF, and OSM (9, 27). In addition, STAT3 is acetylated at the NH_2-terminal residues K49 and K87 on IL6 stimulation (28). The lack of acetylation in KK49/87RR mutants impairs the transcriptional activity of STAT3, preventing its binding with p300, but does not influence its DNA-binding activity (8). Recently, 3 additional lysines have been identified that may undergo acetylation (K679, K707, and K709), which all seem to be implicated in the regulation of STAT3 phosphorylation (21). The growing number of observations and studies concerning STAT3 acetylation suggests that the list of target lysine residues may still be incomplete.

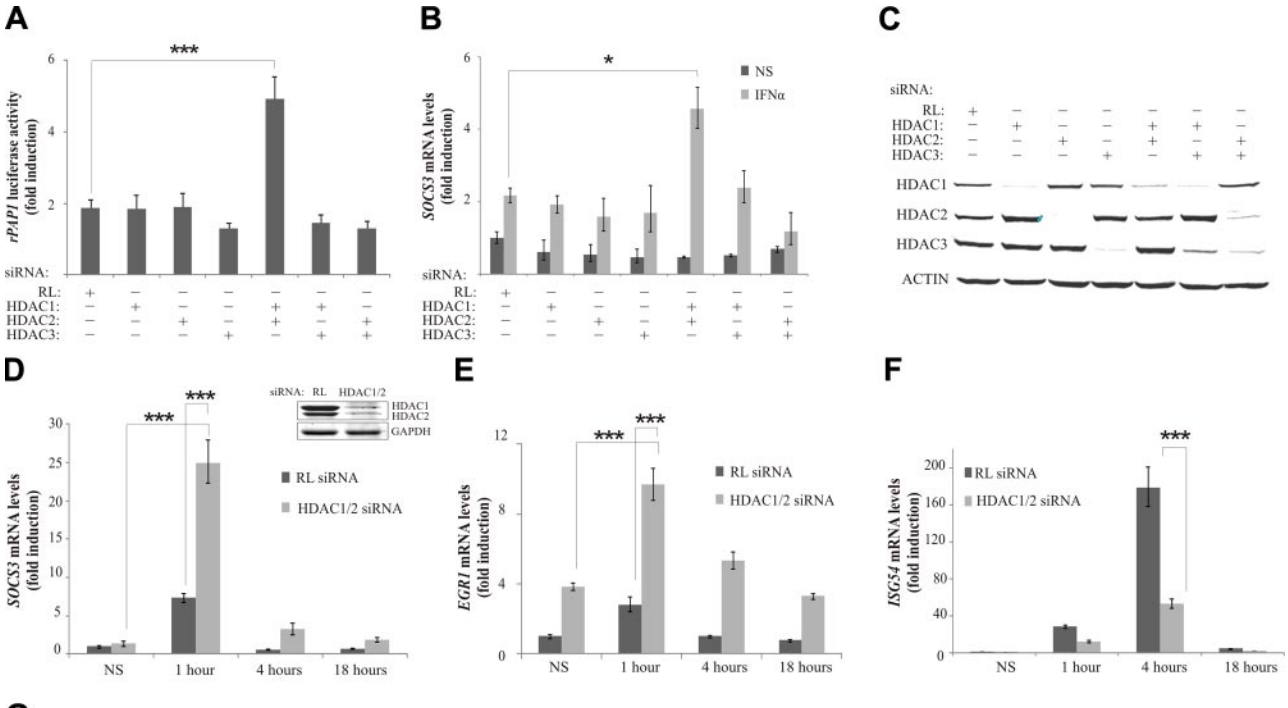

Figure 4. HDAC1 and HDAC2 differentially regulate the transcription of STAT3- and ISGF3-stimulated genes. *A*) Flp-In T-Rex HEK293 cells stably expressing the pXP2d2-rPAP1-luciferase reporter were transfected with a 50 nM solution of siRNAs targeting the *Renilla luciferase* (*RL*, negative control) or with individual or combined siRNAs targeting HDAC1, HDAC2, or HDAC3. At 72 h after transfection, cells were left unstimulated or stimulated with IFNα2 (10 ng/ml) for 24 h before performing the luciferase assay. Luciferase readout is expressed as a ratio between stimulated and unstimulated values. ***$P < 0.001$; *t* test. *B, C*) HEK293T cells were transfected with siRNAs as explained in *A*. At 72 h after transfection, cells were left unstimulated or stimulated with IFNα2 (10 ng/ml) for 1 h. Samples were subjected to qRT-PCR to measure the levels of *SOCS3* mRNA (*B*) and were used to assess silencing efficiency and levels of phospho-STAT3 (*C*). Total lysates were incubated with anti-HDAC1, HDAC2, HDAC3, phospho-STAT3, and STAT3 antibodies. *$P < 0.05$; *t* test. *D–F*) MCF7 cells were transfected with a 50 nM solution of siRNAs targeting RL (negative control) or with siRNAs targeting the HDAC1 and HDAC2. At 72 h after transfection, cells were left unstimulated or stimulated with IFNα2 (10 ng/ml) for the indicated time periods and subjected to qRT-PCR analysis to measure the relative mRNA levels of *SOCS3* (*D*), *EGR1* (*E*) and *ISG54* (*F*). Silencing efficiency was assessed by blotting the total cell extracts with anti-HDAC1, anti-HDAC2, and anti-GAPDH antibodies (*D*). Results are representative of 3 independent experiments. Graphs represent mRNA levels relative to NS, *RL* siRNA-transfected sample. Error bars indicate SD from triplicates. ***$P < 0.001$; 1-way ANOVA with Bonferroni test. *G*) Accumulation of nuclear STAT3 after HDAC1/HDAC2 knockout. MCF7 cells were transfected with either control siRNA (RL siRNA) or HDAC1/HDAC2 siRNA. After 72 h, cells were starved for 16 h. Solvent or IFNα (10 ng/ml) was added for the indicated times, and the localization of STAT3 was assessed by confocal analysis. Confocal immunofluorescence of representative cell fields is shown. HDAC1/2 silencing efficiency is ≥80% and shown in Supplemental Fig. S2.

The reversible lysine acetylation of STAT3 is balanced by the opposite activity of HDACs. Besides their known role in basal gene silencing processes, HDACs are well reported to support a broad-spectrum of regulatory mechanisms, which extend to the regulation of the activity of several transcription factors (29). Recently, also STAT3 has been reported to be regulated by HDAC1, HDAC2, and HDAC3, which associate with STAT3 and contribute to its negative regulation (9–11). Here, we show for the first time that endogenous HDAC1 and HDAC2 may prevent the activity of a transcription factor, STAT3, which had acquired all the hallmarks of an active transcription factor, such as phosphorylation, acetylation, nuclear translocation, and DNA binding. Indeed, cotreatment of the cells with IFNα2 and the HDAC inhibitor TSA, as well as specific HDAC1 and HDAC2 siRNA-mediated silencing, allows the activation of both the STAT3-dependent reporter rPAP1 and the transcription of STAT3-driven endogenous genes. In addition, we show that these two HDACs exert a redundant role in repressing IFNα-activated STAT3, since interfering with the function of only one of the two HDACs does not restore STAT3 activity. This result is in agreement with the fact that HDAC1 and HDAC2 are highly related proteins that share 85% of sequence identity, which probably accounts for the overlapping functions of these two enzymes (30).

Apart from STAT3, CBP was also shown to acetylate several other players of the IFN signaling pathway, such as IFNAR2 and the ISGF3-complex components STAT2 and IRF9, permitting the assembly of the ISGF3 complex and

the transcription of ISGs (31). Furthermore, the activity of HDACs has been clearly shown to be required for ISGF3-dependent transcription (32–34). Treatment with the HDAC inhibitors TSA or valproic acid (VPA) impairs ISGs expression, although the exact molecular mechanisms for this inhibition remain unclear. HDAC inhibitors affect ISGF3 transcriptional activity without altering the tyrosine phosphorylation of STAT1 and STAT2 and without affecting their nuclear translocation or assembly on chromatin. TSA treatment was shown to prevent the IFN-stimulated binding of RNA polymerase II to the *ISG54* promoter (34). On the basis of these observations, it appears likely that HDAC regulation occurs downstream of ISGF3 activation and promoter assembly, but before the recruitment of polymerase II and the onset of transcription.

Our study assigns a broader role for HDACs, in particular, HDAC1 and HDAC2, in the regulation of type I IFN signaling. Indeed, our observation that HDACs actively repress the activity of STAT3, together with their previously described role in supporting ISGF3 signaling, indicates that HDAC1 and HDAC2 differentially modulate STAT activity in response to IFNα: while they are required for the induction of ISGF3-responsive genes, they impair the transcription of STAT3-dependent genes. This leads us to hypothesize the presence of an acetylation-deacetylation switch (**Fig. 5**) that differentially regulates ISGF3- and STAT3-dependent transcription, hence modulating the specificity of the IFNα response. Similar to what has been observed for STAT1 and STAT2, TSA treatment also does not significantly alter the STAT3 phosphorylation status. Intriguingly, interfering with HDAC1 and HDAC2 function seems to affect in a reproducible manner the nuclear-cytoplasmic distribution dynamics of STAT3 after IFNα2 treatment, leading to prolonged nuclear accumulation (Figs. 3*G* and 4*G*). These results are in agreement with the recent observation that HDAC1 interacts with the NH_2-terminal acetylation domain of STAT3 and, as such, controls its subcellular distribution (10). Since IFN-activated STAT3 is recruited at the promoters of *c-FOS* and *SOCS3*, it seems likely that the negative regulatory mechanism exerted by HDACs on its transcriptional activity may occur downstream of DNA binding, as reported for the ISGF3 complex. Further studies will be needed to unveil the molecular mechanisms underlying the differential regulation of ISGF3 and STAT3 activity by HDAC1 and HDAC2. HDACs may act either directly on STAT molecules, modifying their acetylation pattern, or on other transcriptional cofactors, although so far, we could not detect any impairment on histone acetylation or a marked differential cofactor recruitment pattern on the *c-FOS* or *SOCS3* promoters that could explain the absence of transcription (data not shown). Interestingly, priming experiments showed that pretreatment with IFNα2 does not affect the LIF-induced STAT3 transcriptional activity (data not shown), suggesting the coexistence of independent mechanisms of STAT3 transcriptional activation.

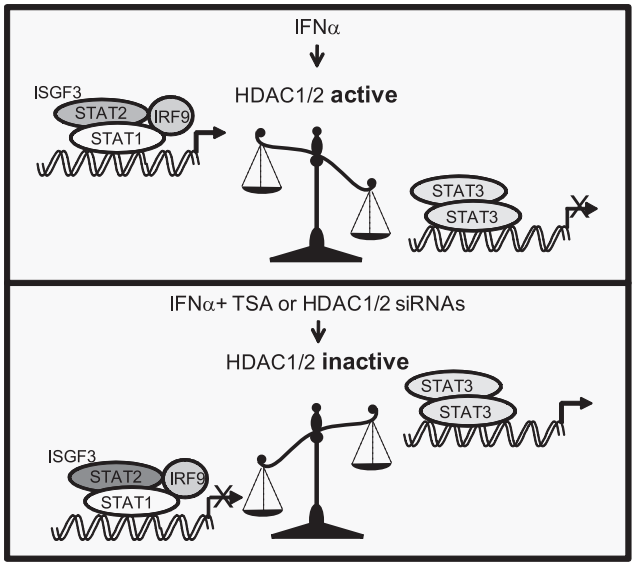

Figure 5. Schematic model of the role of HDAC1/HDAC2 activity in the type I IFN response. Upon IFN stimulation, the activity of HDAC1 and HDAC2 is required for ISGF3-responsive gene transcription, while STAT3-dependent gene activation is impaired. Interfering with HDAC1 and HDAC2 activity, *via* TSA treatment or HDAC1/HDAC2 silencing, enhances the transcription of STAT3-responsive genes and impairs the ISGF3-dependent response.

Although the transcriptional activity of STAT3 is impaired, it is reasonable to assume that its activation must have an effect on the response to IFNs. For instance, activated STAT3 has been proposed to regulate STAT1-dependent signaling by sequestering it in heterodimers and thus attenuating the STAT1-dependent inflammatory response to IFNα (35). In support of this hypothesis, a number of studies have confirmed that STAT1 and STAT3 reciprocally regulate each other's activities, thus contributing to maintain the specificity of cytokine signaling (36–40). Nevertheless, besides its function in the modulation of STAT1 signaling, STAT3 has been reported to have an active role in the IFN-driven apoptotic response in primary murine pro-B cells (41) and an antiviral response in Daudi cells (17), underlining a cell-type dependent role for this transcription factor. Because of these cell-type specific functions, it is expected that the regulation of the transcriptional activity of STAT3 may vary in different cell types. Of note, in contrast with HEK293T and 2fTGH cells, treatment of the breast cancer cell line MCF7 with IFNα2 led to activation of the STAT3-dependent genes *SOCS3* and *EGR1*. Also in this context, HDAC1 and HDAC2 silencing enhanced STAT3-target gene activation, while impaired ISGF3-dependent transcription. In conclusion, we demonstrate that HDAC1 and HDAC2 differently modulate STAT activation in response to IFNα2, as they simultaneously behave as transcription-suppressors, *i.e.*, in the case of STAT3, and as transcription-mediators, *i.e.*, in the case of ISGF3, thus depending on the specific STAT-driven gene promoter context. FJ

The authors thank Dr. Els Pattyn and Annick Verhee for their help in initiating this research project. This work was supported by grants from Ghent University, the Interuniversity Attraction Pole–6 (No. P6:28) and the ReceptEur FP6 Marie-Curie program. K.D.B. is a postdoctoral researcher at the Fonds Wetenschappelijk Onderzoek–Vlaanderen.

REFERENCES

1. Muller, U., Steinhoff, U., Reis, L. F., Hemmi, S., Pavlovic, J., Zinkernagel, R. M., and Aguet, M. (1994) Functional role of type I and type II interferons in antiviral defense. *Science* **264,** 1918–1921
2. Gutterman, J. U. (1994) Cytokine therapeutics: lessons from interferon alpha. *Proc. Natl. Acad. Sci. U. S. A.* **91,** 1198–1205
3. Schindler, C., Levy, D. E., and Decker, T. (2007) JAK-STAT signaling: from interferons to cytokines. *J. Biol. Chem.* **282,** 20059–20063
4. Van Boxel-Dezaire, A. H., Rani, M. R., and Stark, G. R. (2006) Complex modulation of cell type-specific signaling in response to type I interferons. *Immunity* **25,** 361–372
5. Bromberg, J. F. (2001) Activation of STAT proteins and growth control. *Bioessays.* **23,** 161–169
6. Levy, D. E., and Darnell, J. E., Jr. (2002) Stats: transcriptional control and biological impact. *Nat. Rev. Mol. Cell. Biol.* **3,** 651–662
7. Wen, Z., Zhong, Z., and Darnell, J. E., Jr. (1995) Maximal activation of transcription by Stat1 and Stat3 requires both tyrosine and serine phosphorylation. *Cell* **82,** 241–250
8. Hou, T., Ray, S., Lee, C., and Brasier, A. R. (2008) The STAT3 NH2-terminal domain stabilizes enhanceosome assembly by interacting with the p300 bromodomain. *J. Biol. Chem.* **283,** 30725–30734
9. Yuan, Z. L., Guan, Y. J., Chatterjee, D., and Chin, Y. E. (2005) Stat3 dimerization regulated by reversible acetylation of a single lysine residue. *Science* **307,** 269–273
10. Ray, S., Lee, C., Hou, T., Boldogh, I., and Brasier, A. R. (2008) Requirement of histone deacetylase1 (HDAC1) in signal transducer and activator of transcription 3 (STAT3) nucleocytoplasmic distribution. *Nucleic Acids Res.* **36,** 4510–4520
11. Togi, S., Kamitani, S., Kawakami, S., Ikeda, O., Muromoto, R., Nanbo, A., and Matsuda, T. (2009) HDAC3 influences phosphorylation of STAT3 at serine 727 by interacting with PP2A. *Biochem. Biophys. Res. Commun.* **379,** 616–620
12. Bromberg, J. (2002) Stat proteins and oncogenesis. *J. Clin. Invest.* **109,** 1139–1142
13. Bromberg, J. F., Wrzeszczynska, M. H., Devgan, G., Zhao, Y., Pestell, R. G., Albanese, C., and Darnell, J. E., Jr. (1999) Stat3 as an oncogene. *Cell* **98,** 295–303
14. Nusinzon, I., and Horvath, C. M. (2003) Interferon-stimulated transcription and innate antiviral immunity require deacetylase activity and histone deacetylase 1. *Proc. Natl. Acad. Sci. U. S. A.* **100,** 14742–14747
15. Eyckerman, S., Verhee, A., der Heyden, J. V., Lemmens, I., Ostade, X. V., Vandekerckhove, J., and Tavernier, J. (2001) Design and application of a cytokine-receptor-based interaction trap. *Nat. Cell Biol.* **3,** 1114–1119
16. Van Schoubroeck, B., Van Acker, K., Dams, G., Jochmans, D., Clayton, R., Berke, J. M., Lievens, S., Van der Heyden, J., and Tavernier, J. (2012) MAPPIT as a high-throughput screening assay for modulators of protein-protein interactions in HIV and HCV. *Methods Mol. Biol.* **812** In press
17. Graham, F. L., and van der Eb, A. J. (1973) A new technique for the assay of infectivity of human adenovirus 5 DNA. *Virology* **52,** 456–467
18. Witcher, M., Ross, D. T., Rousseau, C., Deluca, L., and Miller, W. H., Jr. (2003) Synergy between all-trans retinoic acid and tumor necrosis factor pathways in acute leukemia cells. *Blood* **102,** 237–245
19. Pierreux, C. E., Nicolas, F. J., and Hill, C. S. (2000) Transforming growth factor beta-independent shuttling of Smad4 between the cytoplasm and nucleus. *Mol. Cell. Biol.* **20,** 9041–9054
20. Hirano, T., Ishihara, K., and Hibi, M. (2000) Roles of STAT3 in mediating the cell growth, differentiation and survival signals relayed through the IL-6 family of cytokine receptors. *Oncogene* **19,** 2548–2556
21. Nie, Y., Erion, D. M., Yuan, Z., Dietrich, M., Shulman, G. I., Horvath, T. L., and Gao, Q. (2009) STAT3 inhibition of gluconeogenesis is downregulated by SirT1. *Nat. Cell Biol.* **11,** 492–500
22. Taplick, J., Kurtev, V., Kroboth, K., Posch, M., Lechner, T., and Seiser, C. (2001) Homo-oligomerisation and nuclear localisation of mouse histone deacetylase 1. *J. Mol. Biol.* **308,** 27–38
23. Yang, W. M., Tsai, S. C., Wen, Y. D., Fejer, G., and Seto, E. (2002) Functional domains of histone deacetylase-3. *J. Biol. Chem.* **277,** 9447–9454
24. Senese, S., Zaragoza, K., Minardi, S., Muradore, I., Ronzoni, S., Passafaro, A., Bernard, L., Draetta, G. F., Alcalay, M., Seiser, C., and Chiocca, S. (2007) Role for histone deacetylase 1 in human tumor cell proliferation. *Mol. Cell. Biol.* **27,** 4784–4795
25. Meraz, M. A., White, J. M., Sheehan, K. C., Bach, E. A., Rodig, S. J., Dighe, A. S., Kaplan, D. H., Riley, J. K., Greenlund, A. C., Campbell, D., Carver-Moore, K., DuBois, R. N., Clark, R., Aguet, M., and Schreiber, R. D. (1996) Targeted disruption of the Stat1 gene in mice reveals unexpected physiologic specificity in the JAK-STAT signaling pathway. *Cell* **84,** 431–442
26. Wang, R., Cherukuri, P., and Luo, J. (2005) Activation of Stat3 sequence-specific DNA binding and transcription by p300/CREB-binding protein-mediated acetylation. *J. Biol. Chem.* **280,** 11528–11534
27. Ohbayashi, N., Ikeda, O., Taira, N., Yamamoto, Y., Muromoto, R., Sekine, Y., Sugiyama, K., Honjoh, T., and Matsuda, T. (2007) LIF- and IL-6-induced acetylation of STAT3 at Lys-685 through PI3K/Akt activation. *Biol. Pharm. Bull.* **30,** 1860–1864
28. Ray, S., Boldogh, I., and Brasier, A. R. (2005) STAT3 NH2-terminal acetylation is activated by the hepatic acute-phase response and required for IL-6 induction of angiotensinogen. *Gastroenterology* **129,** 1616–1632
29. Melnick, A., and Licht, J. D. (2002) Histone deacetylases as therapeutic targets in hematologic malignancies. *Curr. Opin. Hematol.* **9,** 322–332
30. Segre, C. V., and Chiocca, S. (2011) Regulating the regulators: the post-translational code of class I HDAC1 and HDAC2. *J. Biomed. Biotechnol.* 2011:690848
31. Tang, X., Gao, J. S., Guan, Y. J., McLane, K. E., Yuan, Z. L., Ramratnam, B., and Chin, Y. E. (2007) Acetylation-dependent signal transduction for type I interferon receptor. *Cell* **131,** 93–105
32. Chang, H. M., Paulson, M., Holko, M., Rice, C. M., Williams, B. R., Marie, I., and Levy, D. E. (2004) Induction of interferon-stimulated gene expression and antiviral responses require protein deacetylase activity. *Proc. Natl. Acad. Sci. U. S. A.* **101,** 9578–9583
33. Nusinzon, I., and Horvath, C. M. (2006) Positive and negative regulation of the innate antiviral response and beta interferon gene expression by deacetylation. *Mol. Cell. Biol.* **26,** 3106–3113
34. Sakamoto, S., Potla, R., and Larner, A. C. (2004) Histone deacetylase activity is required to recruit RNA polymerase II to the promoters of selected interferon-stimulated early response genes. *J. Biol. Chem.* **279,** 40362–40367
35. Ho, H. H., and Ivashkiv, L. B. (2006) Role of STAT3 in type I interferon responses. Negative regulation of STAT1-dependent inflammatory gene activation. *J. Biol. Chem.* **281,** 14111–14118
36. Regis, G., Pensa, S., Boselli, D., Novelli, F., and Poli, V. (2008) Ups and downs: the STAT1:STAT3 seesaw of interferon and gp130 receptor signalling. *Semin. Cell Dev. Biol.* **19,** 351–359
37. Costa-Pereira, A. P., Tininini, S., Strobl, B., Alonzi, T., Schlaak, J. F., Is'harc, H., Gesualdo, I., Newman, S. J., Kerr, I. M., and Poli, V. (2002) Mutational switch of an IL-6 response to an interferon-gamma-like response. *Proc. Natl. Acad. Sci. U. S. A.* **99,** 8043–8047
38. Qing, Y., and Stark, G. R. (2004) Alternative activation of STAT1 and STAT3 in response to interferon-gamma. *J. Biol. Chem.* **279,** 41679–41685
39. Regis, G., Icardi, L., Conti, L., Chiarle, R., Piva, R., Giovarelli, M., Poli, V., and Novelli, F. (2009) IL-6, but not IFN-gamma, triggers apoptosis and inhibits in vivo growth of human malignant T cells on STAT3 silencing. *Leukemia* **23,** 2102–2108
40. Tanabe, Y., Nishibori, T., Su, L., Arduini, R. M., Baker, D. P., and David, M. (2005) Cutting edge: role of STAT1, STAT3, and STAT5 in IFN-alpha beta responses in T lymphocytes. *J. Immunol.* **174,** 609–613
41. Gamero, A. M., Potla, R., Wegrzyn, J., Szelag, M., Edling, A. E., Shimoda, K., Link, D. C., Dulak, J., Baker, D. P., Tanabe, Y., Grayson, J. M., and Larner, A. C. (2006) Activation of Tyk2 and Stat3 is required for the apoptotic actions of interferon-beta in primary pro-B cells. *J. Biol. Chem.* **281,** 16238–16244

Received for publication July 8, 2011.
Accepted for publication September 15, 2011.

LETTER

doi:10.1038/nature10921

IFITM3 restricts the morbidity and mortality associated with influenza

Aaron R. Everitt[1], Simon Clare[1], Thomas Pertel[2], Sinu P. John[2], Rachael S. Wash[1], Sarah E. Smith[1], Christopher R. Chin[2], Eric M. Feeley[2], Jennifer S. Sims[2], David J. Adams[1], Helen M. Wise[3], Leanne Kane[1], David Goulding[1], Paul Digard[3], Verneri Anttila[1], J. Kenneth Baillie[4,5], Tim S. Walsh[5], David A. Hume[4], Aarno Palotie[1], Yali Xue[1], Vincenza Colonna[1,6], Chris Tyler-Smith[1], Jake Dunning[7], Stephen B. Gordon[8], The GenISIS Investigators*, The MOSAIC Investigators*, Rosalind L. Smyth[9], Peter J. Openshaw[7], Gordon Dougan[1], Abraham L. Brass[2,10] & Paul Kellam[1,11]

The 2009 H1N1 influenza pandemic showed the speed with which a novel respiratory virus can spread and the ability of a generally mild infection to induce severe morbidity and mortality in a subset of the population. Recent *in vitro* studies show that the interferon-inducible transmembrane (IFITM) protein family members potently restrict the replication of multiple pathogenic viruses[1–7]. Both the magnitude and breadth of the IFITM proteins' *in vitro* effects suggest that they are critical for intrinsic resistance to such viruses, including influenza viruses. Using a knockout mouse model[8], we now test this hypothesis directly and find that IFITM3 is essential for defending the host against influenza A virus *in vivo*. Mice lacking *Ifitm3* display fulminant viral pneumonia when challenged with a normally low-pathogenicity influenza virus, mirroring the destruction inflicted by the highly pathogenic 1918 'Spanish' influenza[9,10]. Similar increased viral replication is seen *in vitro*, with protection rescued by the re-introduction of *Ifitm3*. To test the role of IFITM3 in human influenza virus infection, we assessed the *IFITM3* alleles of individuals hospitalized with seasonal or pandemic influenza H1N1/09 viruses. We find that a statistically significant number of hospitalized subjects show enrichment for a minor *IFITM3* allele (SNP rs12252-C) that alters a splice acceptor site, and functional assays show the minor CC genotype IFITM3 has reduced influenza virus restriction *in vitro*. Together these data reveal that the action of a single intrinsic immune effector, IFITM3, profoundly alters the course of influenza virus infection in mouse and humans.

IFITM3 was identified in a functional genomic screen as mediating resistance to influenza A virus, dengue virus and West Nile virus infection *in vitro*[1]. However, the role of the IFITM proteins in antiviral immunity *in vivo* is unknown. Therefore, we infected mice that are homozygous for a disruptive insertion in exon 1 of the *Ifitm3* gene that abolishes its expression[8] (*Ifitm3*$^{-/-}$) with a low-pathogenicity murine-adapted H3N2 influenza A virus (A/X-31). Low-pathogenicity strains of influenza do not normally cause extensive viral replication throughout the lungs, or cause the cytokine dysregulation and death typically seen after infection with highly pathogenic viral strains[9], at the doses used (Fig. 1a). However, low-pathogenicity-infected *Ifitm3*$^{-/-}$ mice became moribund, losing >25% of their original body weight and showing severe signs of clinical illness (rapid breathing, piloerection) 6 days after infection. In comparison, wild-type littermates shed <20% of their original body weight, before fully recovering (Fig. 1a, b). There was little difference in virus replication in the lungs during the first 48 h

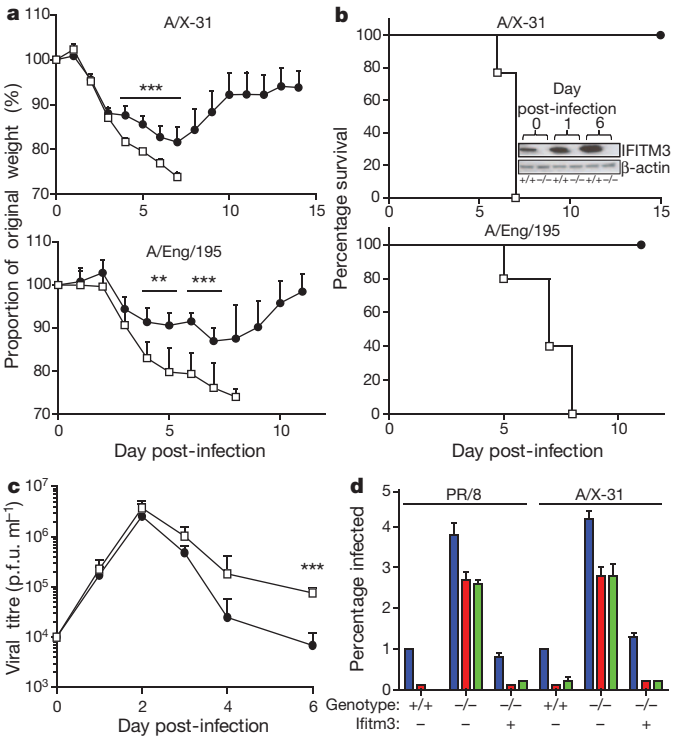

Figure 1 | Influenza A virus replicates to higher levels in *Ifitm3*$^{-/-}$ mice. **a**, **b**, Change in body mass (**a**) and survival (**b**) of wild-type (filled circles) and *Ifitm3*$^{-/-}$ (open squares) mice following intranasal inoculation with A/X-31 and pandemic H1N1/09 Eng/195 influenza ($n > 5$). **b**, Absence of Ifitm3 expression was verified in the *Ifitm3*$^{-/-}$ mice at all time points, but was seen to increase in wild-type mice. **c**, A/X-31 viral load in the lungs of mice ($n > 4$) was calculated over the course of infection by plaque assay. p.f.u., plaque-forming units. *Ifitm3*$^{-/-}$ murine embryonic fibroblasts ($n = 3$ per condition) stably expressing *Ifitm3* (+), or the empty vector (−) were left untreated (blue), or incubated with IFN-α (red) or IFN-γ (green), then challenged with either A/X-31 or PR/8 influenza. **d**, Twelve hours after infection, the cells were assessed for either haemagglutinin expression (PR/8), or nucleoprotein expression (A/X-31) IFITM3 expression was determined to be present (+) or absent (−) by western blotting (Supplementary Fig. 2). Results show means ± s.d. Statistical significance was assessed by Student's *t*-test (**$P < 0.01$; ***$P < 0.001$).

[1]Wellcome Trust Sanger Institute, Wellcome Trust Genome Campus, Hinxton CB10 1SA, UK. [2]Ragon Institute of Massachusetts General Hospital, Massachusetts Institute of Technology, and Harvard University, Charlestown, Massachusetts 02129, USA. [3]Divison of Virology, Department of Pathology, University of Cambridge, Tennis Court Road, Cambridge CB2 1QP, UK. [4]Division of Genetics and Genomics, The Roslin Institute, University of Edinburgh, Roslin EH25 9RG, UK. [5]Department of Critical Care Medicine, University of Edinburgh, Edinburgh EH16 4TJ, UK. [6]Institute of Genetics and Biophysics "A. Buzzati-Traverso", National Research Council (CNR), Naples, Italy. [7]Centre for Respiratory Infection, National Heart and Lung Institute, St Mary's Campus, Imperial College London, W2 1PG, UK. [8]Liverpool School of Tropical Medicine, Pembroke Place, Liverpool L3 5QA, UK. [9]Institute of Translational Medicine, University of Liverpool, Alder Hey Children's Hospital, Liverpool L12 2AP, UK. [10]Gastrointestinal Unit, Massachusetts General Hospital, Boston, Massachusetts 02117, USA. [11]UCL/MRC Centre for Medical Molecular Virology, Department of Infection, University College London, Cleveland Street, London W1T 4JF, UK.

*Lists of participants and their affiliations appear at the end of the paper.

of infection. However, virus persisted and was not cleared as quickly in *Ifitm3*$^{-/-}$ mice, whose lungs contained tenfold higher levels of replicating virus than the wild-type mice at 6 days post-infection (Fig. 1c). No viral RNA was detected in the heart, brain or spleen of infected wild-type or *Ifitm3*$^{-/-}$ mice over the course of infection, revealing that systemic viraemia was not occurring. Full-genome sequencing of virus removed from the lungs of wild-type and *Ifitm3*$^{-/-}$ mice showed no genetic variation. We demonstrated that IFITM3 protein expression after influenza infection was absent in *Ifitm3*$^{-/-}$ mice but increased substantially in wild-type controls (Fig. 1b and Supplementary Fig. 1). Infection of wild-type and *Ifitm3*$^{-/-}$ mice with a human isolate of pandemic influenza A H1N1 (pH1N1/09) resulted in the same severe pathogenicity phenotype in the *Ifitm3*$^{-/-}$ mice (Fig. 1a, b). Mouse embryonic fibroblast (MEF) lines generated from multiple matched littermates demonstrated that *Ifitm3*$^{-/-}$ cells are infected more readily *in vitro*, and lack much of the protective effects of interferon (IFN). Importantly, the stable restoration of IFITM3 conferred wild-type levels of restriction against either the X-31 strain, or the more pathogenic Puerto Rico/8/34 (PR/8) influenza strain (Fig. 1d and Supplementary Fig. 2). In addition to the role of IFITM3 in restriction of high-pathogenicity H5N1 avian influenza[7], we also show that it limits infection by recent human influenza A virus isolates and influenza B virus (Supplementary Fig. 3). Therefore, enhanced pathogenesis to diverse influenza viruses is attributable to loss of *Ifitm3* expression and consequential changes in immune defence of the lungs.

Examination of lung pathology showed fulminant viral pneumonia with substantial damage and severe inflammation in the infected *Ifitm3*$^{-/-}$ mice. Lung pathology was characterized by extensive oedema and red blood cell extravasation, as well as pneumonia, haemorrhagic pleural effusion and multiple, large lesions on all lung lobes (Fig. 2a, b and Supplementary Fig. 4). We note that this pathology is similar to that produced by infection of mice and primates with 1918 H1N1 virus[9–11]. Given the higher viral load in *Ifitm3*$^{-/-}$ mice and increased replication of influenza A virus in *Ifitm3*-deleted cells *in vitro* (Fig. 1d), we examined both viral nucleic acid and protein distribution in the lung. Influenza virus infection penetrated deeper into the lung tissue in *Ifitm3*$^{-/-}$ compared to wild-type mice whose infection was primarily restricted to the bronchioles, with minimal alveolar infection. Influenza virus was detected throughout the entire lung in *Ifitm3*$^{-/-}$ sections, spreading extensively in both bronchioles and alveoli (Fig. 2c). Histopathology showed marked infiltration of cells and debris into the bronchoalveolar space of *Ifitm3*$^{-/-}$ mice (Fig. 2b and Supplementary Fig. 4b). The extent and mechanism of cell damage was investigated by TdT-mediated dUTP nick end labelling (TUNEL) assay, showing widespread cellular apoptosis occurring 6 days post-infection in *Ifitm3*$^{-/-}$ mice, whereas apoptosis in wild-type lungs was very limited (Supplementary Fig. 4c). Together, the *Ifitm3*$^{-/-}$ mouse pathology is consistent with infection by high-pathogenicity strains of influenza A virus, where widespread apoptosis occurs by day 6 post-infection, whereas lungs from low-pathogenicity infections were similar to those of wild-type mice, displaying minimal damage[9,12,13].

Analysis of cell populations resident in the lung tissue on day 6 post-infection showed that *Ifitm3*$^{-/-}$ mice had significantly reduced proportions of CD4$^+$ ($P = 0.004$) and CD8$^+$ T cells ($P = 0.02$) and natural killer (NK) cells ($P = 0.0001$), but an elevated proportion of neutrophils ($P = 0.007$) (Fig. 3a). Despite the extensive cellular infiltration (Supplementary Figs 4b, 5a), the absolute numbers of CD4$^+$ T-lymphocytes in the lungs of the *Ifitm3*$^{-/-}$ mice were also lower and neutrophils increased compared to wild-type mice (Supplementary Fig. 6). The peripheral blood of infected *Ifitm3*$^{-/-}$ mice showed leukopenia (Supplementary Fig. 5c). Blood differential cell counts indicated marked depletion of lymphocytes on day 2 post-infection in the *Ifitm3*$^{-/-}$ mice ($P = 0.04$) (Fig. 3b), reflecting changes observed previously in high-pathogenicity (but not low-pathogenicity) influenza infections in both humans and animal models[9,12,14,15]. Heightened cytokine and chemokine levels are also hallmarks of severe influenza infection, having been observed in both human and animal models[9,16]. We observed exaggerated pro-inflammatory responses in the lungs of *Ifitm3*$^{-/-}$ mice with levels of TNF-α, IL-6, G-CSF and MCP-1 showing the most marked increase (Fig. 3c and Supplementary Fig. 7). This is indicative of the extent of viral spread within the lungs, as TNF-α and IL-6 are released from cells upon infection[17]. Consistent with the immunopathology data above, these changes are comparable in level to those seen with non-H5N1 high-pathogenicity influenza infections[9]. Neutrophil chemotaxis, together with elevated proinflammatory cytokine secretion, has previously been reported as one of the primary causes of acute lung injury[18].

To investigate further the extensive damage observed with low-pathogenicity influenza A virus infection in the absence of IFITM3, we infected both wild-type and *Ifitm3*$^{-/-}$ mice with a PR/8 influenza strain deficient for the multi-functional *NS1* gene (delNS1)[19,20]. NS1 is the primary influenza virus interferon antagonist, with multiple inhibitory effects on host immune pathways[20,21]. We found that delNS1 virus was attenuated in both wild-type and *Ifitm3*$^{-/-}$ mice, and whereas the isogenic PR/8 strain expressing NS1 showed typical high pathogenicity in all mice tested, lower doses of PR/8 influenza (although lethal in both genotypes of mice) caused accelerated weight loss in *Ifitm3*$^{-/-}$ compared to wild-type mice (Supplementary Fig. 8). As delNS1 influenza A virus retains its pathogenicity in IFN-deficient mice[19], this suggests that *Ifitm3*$^{-/-}$ mice can mount an adequate IFN-mediated anti-viral response without extensive morbidity, and that IFITM3 blocking viral replication occurs before NS1-mediated IFN

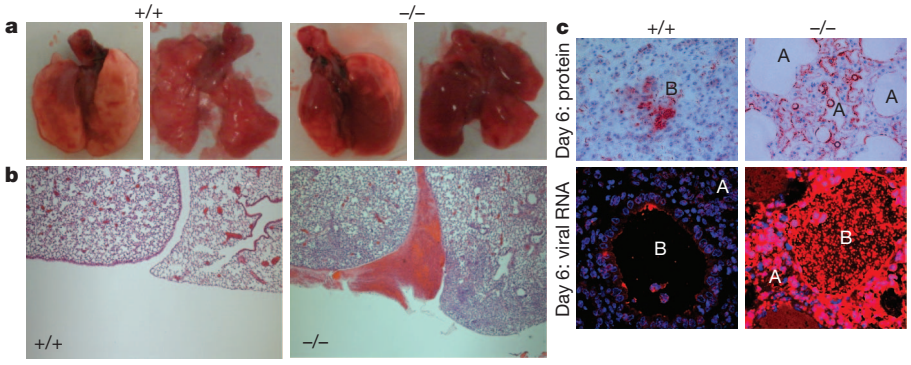

Figure 2 | Pathological examination of infected lungs. **a**, **b**, Wild-type mice showed few visible signs of external damage on lung lobes at day 6 post-infection, whereas *Ifitm3*$^{-/-}$ mice showed several large lesions (**a**, left, ventral view of intact lungs, right, all lobes displayed) resulting from severe oedema and hemorrhagic pleural effusion (**b**), as well as a markedly higher infiltration of cells and proteinaceous debris into the alveoli and bronchioles. **c**, Localization of virus within the lungs on day 6 indicated that virus penetrated deeper and more extensively into the lung tissue in the *Ifitm3*$^{-/-}$ mice, as determined by immunohistochemistry for total influenza protein and detection of virus nucleic acid (virus, red; cell nuclei, blue; A, alveolus; B, bronchiole). Original magnifications were ×5 (**b**) and ×20 (**c**).

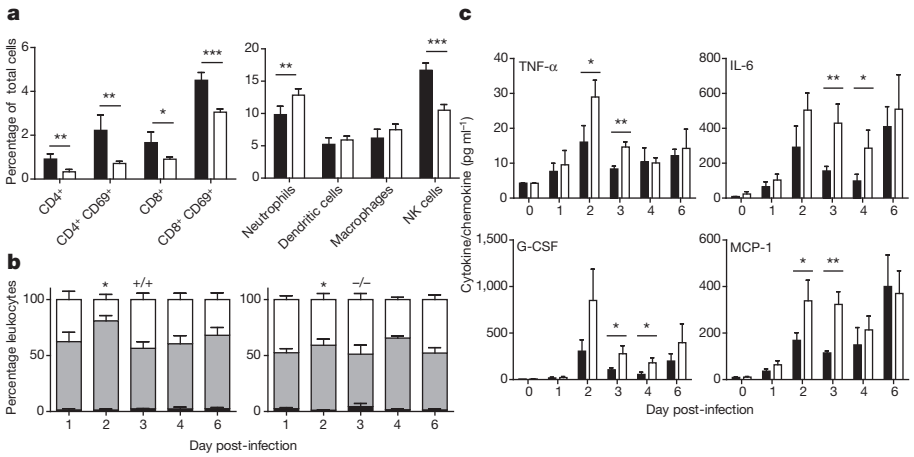

Figure 3 | Altered leukocyte and cytokine response to influenza A infection in *Ifitm3*$^{-/-}$ mice. **a**, Cytometric analysis of proportional resident cell populations in the lungs of mice (+/+, black; −/−, white) showed evidence of lymphopenia in *Ifitm3*$^{-/-}$ mice 6 days post-infection. **b**, Systemic lymphopenia was confirmed through differential analysis of peripheral blood cell counts, which showed a significant depletion of lymphocytes on day 2 post-infection of *Ifitm3*$^{-/-}$ mice (monocytes, black; lymphocytes, grey; polymorphonuclear leukocytes, white). NK, natural killer. **c**, Levels of pro-inflammatory cytokines were also recorded as being elevated in *Ifitm3*$^{-/-}$ lungs over the course of infection (+/+, black; −/−, white). Results show means ± s.d., $n = 5$. Statistical significance was assessed by Student's *t*-test ($*P < 0.05$, $**P < 0.01$, $***P < 0.001$).

antagonism[7]. Therefore, unchecked lung viral replication and an enhanced inflammatory response accounts for the profoundly deleterious effects of viral infection in *Ifitm3*$^{-/-}$ mice.

The human *IFITM3* gene has two exons and is predicted to encode two splice variants that differ by the presence or absence of the first amino-terminal 21 amino acids (Fig. 4a). Currently, 13 non-synonymous, 13 synonymous, one in-frame stop and one splice site acceptor-altering single nucleotide polymorphisms (SNPs) have been reported in the translated *IFITM3* sequence (Supplementary Table 1). Using tests sensitive to recent positive selection, we can find evidence for positive selection on the *IFITM3* locus in human populations acting over the last tens of thousands of years in Africa (Fig. 4b, c). We therefore

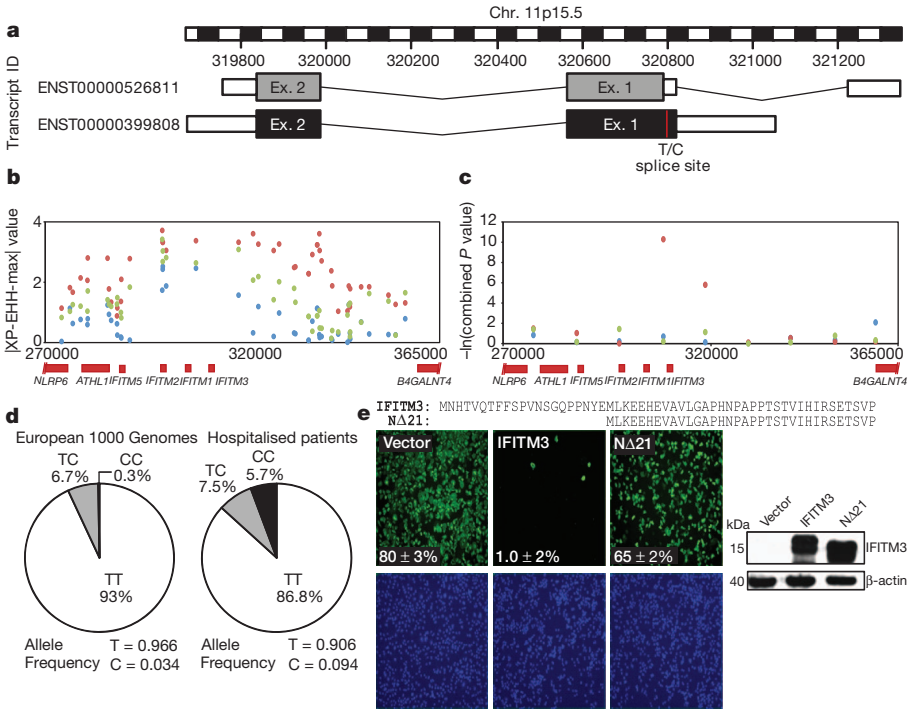

Figure 4 | Single nucleotide polymorphisms of the human *IFITM3* gene. **a**, Multiple single-nucleotide polymorphisms have been identified within the coding region of the human *IFITM3* gene. One such SNP, rs12252 (red), encodes a splice acceptor site altering T/C substitution mutation and may be associated with a truncated protein with an N-terminal 21 amino acid deletion. Therefore two transcripts are predicted to be expressed from the *IFITM3* gene. **b**, **c**, Positive selection analysis using a haplotype-based test, the cross population extended haplotype homozygosity test, maximum value (|XP-EHH-max|, **b**), where data points above 2.7 in the YRI (Africa) (red), 3.9 in the CEU (Europe) (blue) and 5.0 in the CHB+JPT (China and Japan) (green) populations are in the top 1% of values, and using a combination of three allele frequency spectrum-based test statistics (**c**), namely the composite likelihood ratio (CLR)[23–25] on 10-kb windows along chromosome 11 encompassing the *IFITM3* locus. Evidence for positive selection is seen only in the YRI. **d**, Mutations recorded through sequencing of patients hospitalized with influenza virus during the H1N1/09 pandemic showed an overrepresentation of individuals with the C allele at SNP rs12252, relative to matched Europeans. **e**, A549 cells transduced to express either full-length (IFITM3) or truncated (NΔ21) IFITM3 (cell nuclei, blue; virus, green; ×4 magnification) show a reduction in viral restriction when the N-terminal 21 amino acids of IFITM3 are removed, relative to vector controls (Vector). Alignment of the N termini of full-length (IFITM3, top) and truncated IFITM3 (NΔ21, bottom). Values represent the mean of the percentage of infected cells ± s.d. ($n = 3$).

sequenced 1.8 kilobases of the *IFITM3* locus encompassing the exons, intron and untranslated regions from 53 individuals who required admission to hospital as a result of pandemic H1N1/09 or seasonal influenza virus infection in 2009–2010. Of these, 86.8% of patients carried majority alleles for all 28 SNPs in the coding sequence of the gene, but 13.2% possessed known variants. In particular, we discovered over-representation in cases of the synonymous SNP rs12252, wherein the majority T allele is substituted for a minority C allele, which alters the first splice acceptor site and may be associated with the *IFITM3* splice variant (ENST00000526811), which encodes an IFITM3 protein lacking the first 21 amino acids due to the use of an alternative start codon.

The allele frequencies for SNP rs12252 vary in different human populations (Supplementary Table 2). The ancestral (C) allele, reported in chimpanzees, is rare in sub-Saharan African and European populations (derived allele frequency (DAF) 0.093 and 0.026–0.036, respectively), but more frequent in other populations (Supplementary Table 2). SNP rs12252 is notable for its high level of differentiation between Europeans and East Asians, although the fixation index (F_{ST}, a measure of population differentiation) does not reach statistical significance. The genotypes associated with rs12252 in Caucasians hospitalized following influenza infection differ significantly from ethnically matched Europeans in 1000 Genomes sequence data and from genotypes imputed against the June 2011 release of the 1000 Genomes phased haplotypes from the UK, Netherlands and Germany (Wellcome Trust Case Control Consortium 1 (WTCCC1, UK): $P = 0.00006$, Netherlands: $P = 0.00001$, Germany: $P = 0.00007$; Fisher's exact test). Patients' genotypes also depart from Hardy–Weinberg equilibrium ($P = 0.003$), showing an excess of C alleles in this population (Fig. 4d). Principal components analysis of over 100,000 autosomal SNPs showed no evidence of hidden population structure differences between WTCCC controls and a subset of the hospitalised individuals from this study (Supplementary Fig. 9a, b).

To test the functional significance of the IFITM3 rs12252 polymorphism *in vitro*, we confirmed the genotypes of HapMap lymphoblastoid cell lines (LCLs) homozygous for either the majority (TT) or minority (CC) variant IFITM3 alleles (Supplementary Fig. 9c). We next challenged the LCLs with influenza A virus and found that the minority (CC) variant was more susceptible to infection, and this vulnerability correlated with lower levels of IFITM3 protein expression compared to the majority (TT) variant cells (Supplementary Fig. 10). Although we did not detect the IFITM3 splice variant protein (ENST00000526811) in the CC LCLs, we nonetheless investigated the possible significance of its presence by stably expressing the N-terminally truncated (NΔ21) and wild-type proteins to equivalent levels in human A549 lung carcinoma cell lines before infection with influenza A virus (A/WSN/1933 (WSN/33)). We found that cells expressing the NΔ21 protein failed to restrict viral replication when compared to wild-type IFITM3 (Fig. 4e), consistent with previous data showing that the amino-terminal 21 amino acids of IFITM3 are required for attenuation of vesicular stomatitis virus replication *in vitro*[4]. Similar results were obtained using other virulent viral strains (A/California/7/2009 (pH1N1), A/Uruguay/716/2007 (H3N2) and B/Brisbane/60/2008) (Supplementary Fig. 3).

We show here that IFITM3 expression acts as an essential barrier to influenza A virus infection *in vivo* and *in vitro*. The fulminant viral pneumonia that occurs in the absence of IFITM3 arises because of uncontrolled virus replication in the lungs, resulting in profound morbidity. In effect, the host's loss of a single immune effector, IFITM3, transforms a mild infection into one with remarkable severity. Similarly, the enrichment of the rs12252 C-allele in those hospitalized with influenza infections, together with the decreased IFITM3 levels and the increased infection of the CC-allele cells *in vitro*, suggests that IFITM3 also plays a pivotal role in defence against human influenza virus infections. This innate resistance factor is all the more important during encounters with a novel pandemic virus, when the host's acquired immune defences are less effective. Indeed, IFITM3-compromised individuals, and in turn populations with a higher percentage of such individuals, may be more vulnerable to the initial establishment and spread of a virus against which they lack adaptive immunity. In light of its ability to curtail the replication of a broad range of pathogenic viruses *in vitro*, these *in vivo* results suggest that IFITM3 may also shape the clinical course of additional viral infections in favour of the host, and may have done so over human evolutionary history.

METHODS SUMMARY

Mouse infection. Wild-type and *Ifitm3*$^{-/-}$ mice[8] (8–10 weeks of age) were intranasally inoculated with 10^4 p.f.u. of A/X-31 (H3N2) influenza, 200 p.f.u. of A/England/195/09 (pH1N1) influenza, or 50–10^3 p.f.u. of A/PR/8/34 (PR/8) or the PR/8 *NS1* gene deletion mutant (delNS1)[20] (H1N1) in 50 µl of sterile PBS. Mouse weight was recorded daily as well as monitoring for signs of illness. Mice exceeding 25% total weight loss were killed in accordance with UK Home Office guidelines. Infected lungs were collected on days 1–6 post-infection and quantified for viral load by plaque assay and RT-qPCR with primers to influenza matrix 1 protein.

Pathology of infected *Ifitm3*$^{-/-}$ mice. 5-µm sections of paraffin-embedded tissue were stained with haematoxylin and eosin and microscopically examined. Apoptosis was assessed by TUNEL using the TACS XL DAB *In Situ* Apoptosis Detection Kit (R&D Systems). Viral RNA was visualized by QuantiGene viewRNA kit (Affymetrix), with a viewRNA probe set designed to the negative stranded vRNA encoding the *NP* gene of A/X-31 (Affymetrix). Lung tissue was embedded in glycol methacrylate (GMA) and viral antigens stained using M149 polyclonal antibody to influenza A, B (Takara). Single cell suspensions from the lung were characterized by flow cytometry for T-lymphocytes $CD4^+$ or $CD8^+$, T-lymphocytes (activated) $CD4^+CD69^+$ or $CD8^+CD69^+$, neutrophils $CD11b^{hi}CD11c^-Ly6g^+$, dendritic cells $CD11c^+CD11b^{lo}Ly6g^{lo}$ MHC class II high, macrophages $CD11b^+CD11c^+F4/80^{hi}$, natural killer cells $NKp46^+CD4^-CD8^-$.

Sequencing and genetics of human *IFITM3*. The 1.8 kb of human *IFITM3* was amplified and sequenced to identify single nucleotide polymorphisms (SNPs). SNP rs12252 was identified and compared to allele and genotype frequencies from 1000 Genomes sequencing data from different populations including 1000 Genomes imputed. SNP rs12252 allele frequencies were determined in the publicly available genotype data sets of WTCCC1 ($n = 2{,}938$) and previously published data sets genotyped from the Netherlands ($n = 8{,}892$) and Germany ($n = 6{,}253$)[22].

Full Methods and any associated references are available in the online version of the paper at www.nature.com/nature.

Received 7 September 2011; accepted 8 February 2012.
Published online 25 March 2012.

1. Brass, A. L. *et al.* The IFITM proteins mediate cellular resistance to influenza A H1N1 virus, West Nile virus, and dengue virus. *Cell* **139,** 1243–1254 (2009).
2. Jiang, D. *et al.* Identification of five interferon-induced cellular proteins that inhibit West Nile virus and dengue virus infections. *J. Virol.* **84,** 8332–8341 (2010).
3. Yount, J. S. *et al.* Palmitoylome profiling reveals S-palmitoylation-dependent antiviral activity of IFITM3. *Nature Chem. Biol.* **6,** 610–614 (2010).
4. Weidner, J. M. *et al.* Interferon-induced cell membrane proteins, IFITM3 and tetherin, inhibit vesicular stomatitis virus infection via distinct mechanisms. *J. Virol.* **84,** 12646–12657 (2010).
5. Huang, I. C. *et al.* Distinct patterns of IFITM-mediated restriction of filoviruses, SARS coronavirus, and influenza A virus. *PLoS Pathog.* **7,** e1001258 (2011).
6. Schoggins, J. W. *et al.* A diverse range of gene products are effectors of the type I interferon antiviral response. *Nature* **472,** 481–485 (2011).
7. Feeley, E. M. *et al.* IFITM3 inhibits influenza A virus infection by preventing cytosolic entry. *PLoS Pathog.* **7,** e1002337 (2011).
8. Lange, U. C. *et al.* Normal germ line establishment in mice carrying a deletion of the *Ifitm/Fragilis* gene family cluster. *Mol. Cell. Biol.* **28,** 4688–4696 (2008).
9. Belser, J. A. *et al.* Pathogenesis of pandemic influenza A (H1N1) and triple-reassortant swine influenza A (H1) viruses in mice. *J. Virol.* **84,** 4194–4203 (2010).
10. Tumpey, T. M. *et al.* Characterization of the reconstructed 1918 Spanish influenza pandemic virus. *Science* **310,** 77–80 (2005).
11. Kobasa, D. *et al.* Aberrant innate immune response in lethal infection of macaques with the 1918 influenza virus. *Nature* **445,** 319–323 (2007).
12. Tumpey, T. M., Lu, X. H., Morken, T., Zaki, S. R. & Katz, J. M. Depletion of lymphocytes and diminished cytokine production in mice infected with a highly virulent influenza A (H5N1) virus isolated from humans. *J. Virol.* **74,** 6105–6116 (2000).
13. Kobasa, D. *et al.* Enhanced virulence of influenza A viruses with the haemagglutinin of the 1918 pandemic virus. *Nature* **431,** 703–707 (2004).
14. Maines, T. R. *et al.* Pathogenesis of emerging avian influenza viruses in mammals and the host innate immune response. *Immunol. Rev.* **225,** 68–84 (2008).
15. Perrone, L. A., Plowden, J. K., Garcia-Sastre, A., Katz, J. M. & Tumpey, T. M. H5N1 and 1918 pandemic influenza virus infection results in early and excessive infiltration of macrophages and neutrophils in the lungs of mice. *PLoS Pathog.* **4,** e1000115 (2008).

16. Fukuyama, S. & Kawaoka, Y. The pathogenesis of influenza virus infections: the contributions of virus and host factors. *Curr. Opin. Immunol.* **23,** 481–486 (2011).
17. Julkunen, I. *et al.* Inflammatory responses in influenza A virus infection. *Vaccine* **19,** S32–S37 (2000).
18. Yum, H. K. *et al.* Involvement of phosphoinositide 3-kinases in neutrophil activation and the development of acute lung injury. *J. Immunol.* **167,** 6601–6608 (2001).
19. García-Sastre, A. *et al.* Influenza A virus lacking the NS1 gene replicates in interferon-deficient systems. *Virology* **252,** 324–330 (1998).
20. Hale, B. G., Randall, R. E., Ortin, J. & Jackson, D. The multifunctional NS1 protein of influenza A viruses. *J. Gen. Virol.* **89,** 2359–2376 (2008).
21. Billharz, R. *et al.* The NS1 protein of the 1918 pandemic influenza virus blocks host interferon and lipid metabolism pathways. *J. Virol.* **83,** 10557–10570 (2009).
22. Anttila, V. *et al.* Genome-wide association study of migraine implicates a common susceptibility variant on 8q22.1. *Nature Genet.* **42,** 869–873 (2011).
23. Tajima, F. Statistical method for testing the neutral mutation hypothesis by DNA polymorphism. *Genetics* **123,** 585–595 (1989).
24. Fay, J. C. & Wu, C.-I. Hitchhiking under positive Darwinian selection. *Genetics* **155,** 1405–1413 (2000).
25. Nielsen, R. *et al.* Genomic scans for selective sweeps using SNP data. *Genome Res.* **15,** 1566–1575 (2005).

Supplementary Information is linked to the online version of the paper at www.nature.com/nature.

Acknowledgements We would like to thank C. Brandt for maintaining mouse colony health and well-being and T. Hussell for provision of A/X-31 virus. We also thank D. Gurdasani and M. Sandhu for statistical analysis of genotype frequencies. We also thank M. Hu and I. Gallego Romero for calculating genome-wide selection statistics. This work was supported by the Wellcome Trust. The MOSAIC work was supported by Imperial's Comprehensive Biomedical Research Centre (cBRC), the Wellcome Trust (090382/Z/09/Z) and Medical Research Council UK. The GenISIS work was supported by the Chief Scientist Office (Scotland). A.L.B. is the recipient of a Charles H. Hood Foundation Child Health Research Award, and is supported by grants from the Phillip T. and Susan M. Ragon Institute Foundation, the Bill and Melinda Gates Foundation's Global Health Program and the National Institute of Allergy and Infectious Diseases (R01AI091786). J.K.B. is supported by a Wellcome Trust Clinical Lectureship (090385/Z/09/Z) through the Edinburgh Clinical Academic Track (ECAT). We acknowledge the assistance of K. Alshafi, E. Bailey, A. Bermingham, M. Berry, C. Bloom, E. Brannigan, S. Bremang, J. Clark, M. C. Cox, M. Cross, L. A. Cumming, S. Dyas, J. England-Smith, J. Enstone, D. Ferreira, N. Goddard, A. Godlee, S. Gormley, M. Guiver, M. O. Hassan-Ibrahim, H. Hill, P. Holloway, K. Hoschler, G. Houghton, F. Hughes, R. R. Israel, A. Jepson, K. D. Jones, W. P. Kelleher, M. Kidd, K. Knox, A. Lackenby, G. Lloyd, H. Longworth, M. Minns, S. Mookerjee, S. Mt-Isa, D. Muir, A. Paras, V. Pascual, L. Rae, S. Rodenhurst, F. Rozakeas, E. Scott, E. Sergi, N. Shah, V. Sutton, J. Vernazza, A. W. Walker, C. Wenden, T. Wotherspoon, A. D. Wright, F. Wurie and the clinical and laboratory staff of the Alder Hey Children's NHS Foundation Trust, Brighton & Sussex University Hospitals NHS Trust, Central Manchester University Hospitals NHS Foundation Trust, Chelsea and Westminster Hospital NHS Foundation Trust, Alder Hey Children's Hospital and Liverpool School of Tropical Medicine, Health Protection Agency Microbiology Services Colindale, Imperial College Healthcare NHS Trust, Liverpool Women's NHS Foundation Trust, Royal Liverpool and Broadgreen University Hospitals NHS Trust, Royal Brompton and Harefield NHS Foundation Trust, The Roslin Institute, Edinburgh, University Hospitals Coventry and Warwickshire NHS Trust. The MOSAIC consortium was supported by several Comprehensive Local Research Networks (CLRNs), the National Institute for Health Research (NIHR), UK, and by the Biomedical Research Centre (BRC) and Unit (BRU) funds. Finally, we thank all patients and their relatives for their generous agreement to inclusion in this study.

Author Contributions A.R.E., G.D., A.L.B. and P.K. designed the study; A.R.E., P.J.O., G.D., A.L.B. and P.K. wrote the manuscript; A.R.E. performed experiments and analysed data; S.C. designed experiments and performed all live animal work; S.E.S. sequenced and analysed the human *Ifitm3* gene; R.S.W., S.E.S., C.R.C., J.S.S., S.P.J., T.P., E.M.F., A.L.B. and L.K. performed experiments; D.J.A. created the genetically-modified *Ifitm3*$^{-/-}$ mouse line; H.M.W. and P.D. made the influenza virus strains and advised on virology; D.G. performed microscopy; Y.X., V.C. and C.T.-S. performed positive selection analyses; V.A. and A.P. performed imputation and analysis of 1000 Genomes data; E.M.F., C.R.C. and A.L.B. performed *in vitro* viewRNA experiments; recruitment and selection of hospitalised individuals infected with influenza virus was co-ordinated by J.K.B., D.A.H. and T.S.W. (GenISIS) and R.L.S., S.B.G., J.D., J.K.B., D.A.H. and P.J.O. (MOSAIC).

Author Information *IFITM3* sequences are deposited in GenBank under the accession numbers JQ610570–JQ610621. Reprints and permissions information is available at www.nature.com/reprints. The authors declare no competing financial interests. Readers are welcome to comment on the online version of this article at www.nature.com/nature. Correspondence and requests for materials should be addressed to P.K. (pk5@sanger.ac.uk) or A.L.B. (abrass@partners.org).

MOSAIC Core Investigators

Benaroya Research Institute, USA D. Chaussabel[1]; **Gartnavel General Hospital, Greater Glasgow, UK** W. E. Adamson[2], W. F. Carman[2]; **Health Protection Agency, UK** C. Thompson[3], M. C. Zambon[3]; **Imperial College London, UK** P. Aylin[4], D. Ashby[4], W. S. Barclay[4], S. J. Brett[4], W. O. Cookson[4], L. N. Drumright[4], J. Dunning[4], R. A. Elderfield[4], L. Garcia-Alvarez[4], B. G. Gazzard[4], M. J. Griffiths[4], M. S. Habibi[4], T. T. Hansel[4], J. A. Herberg[4], A. H. Holmes[4], T. Hussell[4], S. L. Johnston[4], O. M. Kon[4], M. Levin[4], M. F. Moffatt[4], S. Nadel[4], P. J. Openshaw[4], J. O. Warner[4]; **Liverpool School of Tropical Medicine, UK** S. J. Aston[5], S. B. Gordon[5]; **National Institute for Medical Research, UK** A. Hay[6], J. McCauley[6], A. O'Garra[6]; **Roche, Nutley, USA** J. Banchereau[7]; **University College London, UK** A. Hayward[8], P. Kellam[8]; **University of Edinburgh, UK** J. K. Baillie[9], D. A. Hume[9], P. Simmonds[9]; **University of Liverpool, UK** P. S. McNamara[10], M. G. Semple[10], R. L. Smyth[10]; **University of Nottingham, UK** J. S. Nguyen-Van-Tam[11]; **University of Oxford, UK** L.-P. Ho[12], A. J. McMichael[12]; **Wellcome Trust Sanger Institute, UK** P. Kellam[13].

GenISIS Investigators

Critical Care Medicine, University of Edinburgh K. Everingham[14], H. Dawson[14], D. Hope[14], P. Ramsay[14], T. S. Walsh (Local Lead Investigator)[14]; **Generation Scotland, University of Edinburgh Molecular Medicine Centre** A. Campbell[15], S. Kerr[15]; **Intensive Care National Audit & Research Centre, London** D. Harrison[16], K. Rowan[16]; **Intensive Care Unit, Aberdeen Royal Infirmary** J. Addison[17], N. Donald[17], S. Galt[17], D. Noble[17], J. Taylor[17], N. Webster (Local Lead Investigator)[17]; **Intensive Care Unit, Ayr Hospital** I. Taylor (Local Lead Investigator)[18]; **Intensive Care Unit, Borders General Hospital, Melrose** J. Aldridge (Local Lead Investigator)[19], R. Dornan[19], C. Richard[19]; **Intensive Care Unit, Crosshouse Hospital, Kilmarnock** D. Gilmour[20], R. Simmons (Local Lead Investigator)[20], R. White (Local Lead Investigator)[20]; **Intensive Care Unit, Dumfries and Galloway Royal Infirmary** C. Jardine[21], D. Williams (Local Lead Investigator)[21]; **Intensive Care Unit, Glasgow Royal Infirmary** M. Booth (Local Lead Investigator)[22], T. Quasim[22]; **Intensive Care Unit, Hairmyres Hospital, Lanarkshire** V. Watson[23]; **Intensive Care Unit, Inverclyde Royal Hospital, Greenock** P. Henry[24], F. Munro[24]; **Intensive Care Unit, Monklands Hospital, Airdrie** L. Bell[25], J. Ruddy (Local Lead Investigator)[25]; **Intensive Care Unit, Ninewells Hospital, Dundee** S. Cole (Local Lead Investigator)[26], J. Southward[26]; **Intensive Care Unit, Queen Margaret Hospital, Dunfermline** P. Allcoat[27], S. Gray[27], M. McDougall (Local Lead Investigator)[27]; **Intensive Care Unit, Raigmore Hospital, Inverness** J. Matheson[28], J. Whiteside (Local Lead Investigator)[28]; **Intensive Care Unit, Royal Alexandra Hospital, Paisley** D. Alcorn[29], K. Rooney (Local Lead Investigator)[29], R. Sundaram[29]; **Intensive Care Unit, Southern General Hospital, Glasgow** G. Imrie (Local Lead Investigator)[30]; **Intensive Care Unit, St John's Hospital, Livingston** J. Bruce[31], K. McGuigan[31], S. Moultrie (Local Lead Investigator)[31]; **Intensive Care Unit, Stirling Royal Infirmary** C. Cairns (Local Lead Investigator)[32], J. Grant[32], M. Hughes[32]; **Intensive Care Unit, Stobhill Hospital, Glasgow** C. Murdoch (Local Lead Investigator)[33]; **Intensive Care Unit, Victoria Hospital, Glasgow** A. Davidson (Local Lead Investigator)[34]; **Intensive Care Unit, Western General Hospital, Edinburgh** G. Harris[35], R. Paterson[35], C. Wallis (Local Lead Investigator)[35]; **Intensive Care Unit, Western Infirmary, Glasgow** S. Binning (Local Lead Investigator)[36], M. Pollock[36]; **Wellcome Trust Clinical Research Facility, Edinburgh** J. Antonelli[37], A. Duncan[37], J. Gibson[37], C. McCulloch[37], L. Murphy[37]; **Roslin Institute, University of Edinburgh** C. Haley[38], G. Faulkner[38], T. Freeman[38], D. A. Hume[38] & J. K. Baillie (Principal Investigator)[38].

[1]Benaroya Research Institute, 1201 9th Avenue, Seattle, Washington 98101-2795, USA. [2]West of Scotland Specialist Virology Centre, Gartnavel General Hospital, Glasgow and Clyde Health Board, 1053 Great Western Road, Glasgow G12 0YN, UK. [3]Health Protection Agency, Microbiology Services Colindale, 61 Colindale Avenue, London NW9 5EQ, UK. [4]Imperial College London, St Mary's Campus, Norfolk Place, London W2 1PG, UK. [5]Liverpool School of Tropical Medicine, Pembroke Place, Liverpool L3 5QA, UK. [6]National Institute for Medical Research (NIMR), The Ridgeway, London NW7 1AA, UK. [7]Roche, 340 Kingsland Street, Nutley, New Jersey 07110-1199, USA. [8]University College London, Gower Street, London, WC1E 6BT, UK. [9]The Roslin Institute and R(D)SVS, University of Edinburgh, Easter Bush, Midlothian EH25 9RG, UK. [10]Department of Women's and Children's Health, Institute of Translational Medicine, University of Liverpool, Alder Hey Children's Hospital, Liverpool L12 2AP, UK. [11]Epidemiology and Public Health, University of Nottingham, Clinical Sciences Building, City Hospital, Nottingham NG5 1PB, UK. [12]The Weatherall Institute of Molecular Medicine, University of Oxford, John Radcliffe Hospital, Oxford OX3 9DS, UK. [13]Wellcome Trust Sanger Institute, Wellcome Trust Genome Campus, Hinxton, Cambridge CB10 1SA, UK. [14]Department of Critical Care Medicine, The Queen's Medical Research Institute, College of Medicine and Veterinary Medicine, University of Edinburgh, 47 Little France Drive, Edinburgh EH16 4TJ, UK [15]Generation Scotland, University of Edinburgh, Molecular Medicine Centre, Western General Hospital, Crewe Road South, Edinburgh EH4 2XU, UK. [16]Intensive Care National Audit & Research Centre, Tavistock House, Tavistock Square, London WC1H 9HR, UK. [17]Intensive Care Unit, Aberdeen Royal Infirmary, Foresterhill, Aberdeen AB25 2ZN, UK. [18]Intensive Care Unit, Ayr Hospital, Dallmellington Road, Ayr KA6 6DX, UK. [19]Intensive Care Unit, Borders General Hospital, Melrose TD6 9BS, UK. [20]Intensive Care Unit, Crosshouse Hospital, Kilmarnock KA2 0BE, UK. [21]Intensive Care Unit, Dumfries and Galloway Royal Infirmary, Dumfries DG1 4AP, UK. [22]Intensive Care Unit, Glasgow Royal Infirmary, Glasgow G4 0SF, UK. [23]Intensive Care Unit, Hairmyres Hospital, Lanarkshire G75 8RG, UK. [24]Intensive Care Unit, Inverclyde Royal Hospital, Greenock PA16 0XN, UK. [25]Intensive Care Unit, Monklands Hospital, Airdrie ML6 0JS, UK. [26]Intensive Care Unit, Ninewells Hospital, Dundee DD1 9SY, UK. [27]Intensive Care Unit, Queen Margaret Hospital, Dunfermline KY12 0SU, UK. [28]Intensive Care Unit, Raigmore Hospital, Inverness IV2 3UJ, UK. [29]Intensive Care Unit, Royal Alexandra Hospital, Paisley PA2 9PN, UK. [30]Intensive Care Unit, Southern General Hospital, Glasgow G51 4TF, UK. [31]Intensive Care Unit, St John's Hospital, Livingston EH54 6PP, UK. [32]Intensive Care Unit, Stirling Royal Infirmary, Stirling FK8 2AU, UK. [33]Intensive Care Unit, Stobhill Hospital, Glasgow G21 3UW, UK. [34]Intensive Care Unit, Victoria Hospital, Glasgow G42 9TY, UK. [35]Intensive Care Unit, Western General Hospital, Crewe Road South, Edinburgh EH4 2XU, UK. [36]Intensive Care Unit, Western Infirmary, Glasgow G11 6NT, UK. [37]Wellcome Trust Clinical Research Facility, Western General Hospital, Crewe Road South, Edinburgh EH4 2XU, UK. [38]Division of Genetics and Genomics, The Roslin Institute, University of Edinburgh, Easter Bush, Midlothian EH25 9RG, UK.

METHODS

Mouse infection. Background-matched wild-type (>95% C57BL/6) and *Ifitm3*$^{-/-}$ mice[8] 8–10 weeks of age were maintained in accordance with UK Home Office regulations, UK Animals Scientific Procedures Act 1986 under the project licence PPL80/2099. This licence was reviewed by The Wellcome Trust Sanger Institute Ethical Review Committee. Groups of >5 isofluorane-anaesthetized mice of both genotype were intranasally inoculated with 10^4 p.f.u. of A/X-31 influenza in 50 µl of sterile PBS. In some experiments A/X-31 was substituted with 200 p.f.u. of A/England/195/09 influenza, or 50–10^3 p.f.u. of A/PR/8/34 (PR/8) or an otherwise isogenic virus with a deletion of the *NS1* gene (delNS1)[19], made as described[26]. Their weight was recorded daily and they were monitored for signs of illness. Mice exceeding 25% total weight loss were killed in accordance with UK Home Office guidelines. Littermate controls were used in all experiments.

Influenza virus quantification. Lungs from five mice per genotype were collected on days 1, 2, 3, 4 and 6 post-infection, weighed and homogenized in 5% weight/volume (w/v) of Leibovitz's L-15 medium (Invitrogen) containing antibiotic-antimycotic (Invitrogen). Samples were quantified for viral load by plaque assay in tenfold serial dilutions on Madin–Darby canine kidney (MDCK) cell monolayers overlaid with 1% Avicell medium[27]. Lungs were subjected to two freeze-thaw cycles before titration. Virus was also quantified by quantitative PCR with reverse transcription (qRT–PCR), wherein RNA was first extracted from lung, heart, brain and spleen using the RNeasy Mini Plus Kit (Qiagen). Purified RNA was normalized by mass and quantified with SYBR Green (Qiagen) using the manufacturer's instructions and 0.5 µM primers for influenza matrix 1 protein (*M1*) forward: 5′-TGA GTCTTCTAACCGAGGTC-3′, reverse: 5′-GGTCTTGTCTTTAGCCATTCC-3′ (Sigma-Aldrich) and mouse β-actin (*Actb*) forward: 5′-CTAAGGCCAACCGTG AAAAG-3′, reverse: 5′-ACCAGAGGCATACAGGGACA-3′. qPCR was performed on a StepOnePlus machine (Applied Biosystems) and analysed with StepOne software v2.1 (Applied Biosystems).

Western blotting. Lungs were homogenized in 5% w/v of Tissue Protein Extraction Reagent (Thermo Scientific) containing cOmplete Protease Inhibitor (Roche). Total protein was quantified by BCA assay (Thermo Scientific) and was normalized before loading into wells. Proteins were visualized with the following indicated primary antibodies: anti-mouse IFITM2 rabbit polyclonal was purchased from Santa Cruz Biotechnology (catalogue no. sc-66828); anti-Fragilis (Ifitm3) rabbit polyclonal antibody was from Abcam (catalogue no. ab15592). The IFITM3 and NΔ21 western blot using the A549 stable cell lines were probed with the anti-IFITM1 antibody from Prosci (catalogue no. 5807), which recognizes a conserved portion of the IFITM1, IFITM2 and IFITM3 proteins which is still present even in the absence of the first twenty one N-terminal amino acids. The LCL blots (including the A549 cell line lysate controls) were probed with either an antibody which is specific for the N terminus of IFITM3 (rabbit anti-IFITM3 (N-terminal amino acids 8–38) (Abgent, catalogue no. AP1153a)), or with anti-IFITM1 antibody from Prosci (catalogue no. 5807), as well as rabbit anti-MX1 (Proteintech, catalogue no. 13750-1-AP) and mouse anti-GAPDH (clone GAPDH-71.1) (Sigma, catalogue no. G8795). For the LCL immunoblots all antibodies were diluted in DPBS (Sigma) containing 0.1% Tween 20 (Sigma) and 5% non-fat dried milk (Carnation) and incubated overnight at 4 °C. All primary antibodies were consequently bound to the corresponding species-appropriate horseradish peroxidase-conjugated secondary antibodies (Dako). Actin antibody was purchased from either Abcam or Sigma, mouse monoclonal, catalogue no. A5316.

Pathological examination. 5-µm sections of paraffin-embedded tissue were stained with haematoxylin and eosin (Sigma-Aldrich) and were examined and scored twice, once by a pathologist under blinded conditions. The TUNEL assay for apoptosis was conducted using the TACS XL DAB *In Situ* Apoptosis Detection Kit (R&D Systems).

Immunofluorescent tissue staining: protein. Lung tissue was embedded in glycol methacrylate (GMA) to visualize the spread of viral protein, as described previously[28]. Briefly, 2-µm sections were blocked with 0.1% sodium azide and 30% hydrogen peroxide followed by a second block of RPMI 1640 (Invitrogen) containing 10% fetal calf serum (Sigma-Aldrich) and 1% bovine serum albumin (Invitrogen). Viral antigen was stained using M149 polyclonal antibody to influenza A, B (Takara) and visualized with a secondary goat anti-rabbit antibody conjugated to alkaline phosphatase (Dako). Sections were counterstained with haematoxylin (Sigma-Aldrich). Murine IFITM1 and IFITM3 protein expression in lung sections from either uninfected mice, or those 2 days post-infection with A/X-31, were immunostained with either anti-IFITM1 antibody (Abcam, catalogue no. ab106265) or anti-fragilis (anti-Ifitm3) rabbit polyclonal antisera (Abcam, catalogue no. ab15592). Sections were also stained for DNA with Hoechst 33342 (Sigma).

Immunofluorescent staining: RNA. Viral RNA was visualized in 5-µm paraffin-embedded sections using the QuantiGene viewRNA kit (Affymetrix). Briefly, sections were rehydrated and incubated with proteinase K. They were subsequently incubated with a viewRNA probe set designed against the negative stranded viral RNA encoding the *NP* gene of A/X-31 (Affymetrix). The signal was amplified before incubation with labelled probes and visualized.

Flow cytometry. Single-cell suspensions were generated by passing lungs twice through a 100-µm filter before lysing red blood cells with RBC lysis buffer (eBioscience) and assessing for cell viability via Trypan blue exclusion. Cells were characterized by flow cytometry as follows: T-lymphocytes $CD4^+$ or $CD8^+$, T-lymphocytes (activated) $CD4^+CD69^+$ or $CD8^+CD69^+$, neutrophils $CD11b^{hi}CD11c^-Ly6g^+$, dendritic cells $CD11c^+CD11b^{lo}Ly6g^{lo}$ MHC class II high, macrophages $CD11b^+CD11c^+F4/80^{hi}$, natural killer cells $NKp46^+CD4^-CD8^-$. All antibodies (Supplementary Table 3) were from BD Bioscience, except CD69 and F4/80, which were from AbD Serotec. Samples were run on a FACSAria II (BD Bioscience) and visualized using FlowJo 7.2.4. Data were analysed statistically and graphed using Prism 5.0 (GraphPad Software).

Peripheral leukocyte analysis. Mice ($n = 3$ per genotype per day) were bled on days 0, 1, 2, 3, 4 and 6 by tail vein puncture. Leukocyte counts were determined by haemocytometer, whereas blood cell differential counts were calculated by counting from duplicate blood smears stained with Wright–Giemsa stain (Sigma-Aldrich). At least 100 leukocytes were counted per smear. All blood analyses were conducted in a blinded fashion. Data were analysed statistically and graphed using Prism 5.0 (GraphPad Software).

Cytokine/chemokine analysis. Lungs were collected and homogenized on days 0, 1, 2, 3, 4 and 6 post-infection from four mice of each genotype. G-CSF, GM-CSF, IFN-γ, IL-10, IL-1α, IL-1β, IL-2, IL-4, IL-5, IL-6, IL-9, IP-10, KC-like, MCP-1, MIP-1α, RANTES and TNF-α were analysed using a mouse antibody bead kit (Millipore) according to the manufacturer's instructions on a Luminex FlexMAP3D. Results were analysed and quality control checked using Masterplex QT 2010 and Masterplex Readerfit 2010 (MiraiBio). Data were analysed statistically and graphed using Prism 5.0 (GraphPad Software).

Murine embryonic fibroblast generation, transduction and infectivity assays. Adult *Ifitm3*$^{-/-}$ mice[8] were intercrossed and fibroblasts (MEFs) were derived from embryos at day 13.5 of gestation, as described previously[1]. MEFs were genotyped by PCR (Thermo-Start *Taq* DNA Polymerase, ABgene) on embryo tail genomic DNA using primers and the cycle profile described previously[8] to detect the presence of the wild-type allele (450 base pairs band) and the targeted/knock-out allele (650 bp band). MEFs were cultured in DMEM containing 10% FBS, 1× MEM essential amino acids, 1× 2-mercapto-ethanol (Gibco). MEFs were transduced with vesicular stomatitis virus G (VSV-G) pseudotyped retroviruses expressing either the empty vector control (pQXCIP, Clontech), or one expressing *Ifitm3*, as previous described[1]. After puromycin selection the respective cell lines were challenged with either A/X-31 virus (multiplicity of infection (m.o.i.) 0.3–0.4) or PR/8 (m.o.i. 0.4). For PR/8 infections, after 12 h the media was removed and the cells were then fixed with 4% formalin and stained with purified anti-haemagglutinin monoclonal antibody (Hybridoma HA36-4-5.2, Wistar Institute). For A/X-31 experiments, cells were processed comparably as above, but in addition were permeabilized, followed by immunostaining for NP expression (NP (clone H16-L10-4R5) mouse monoclonal (Millipore MAB8800)). Both sets of experiments were completed using an Alexa Fluor 488 goat anti-mouse secondary antibody at 1:1,000 (A11001, Invitrogen). The cells were imaged on an automated Image Express Micro microscope (Molecular Devices), and images were analysed using the MetaMorph Cell Scoring software program (Molecular Devices). Cytokines: cells were incubated with cytokines for 24 h before viral infection. Murine interferon α (PBL Interferon Source, catalogue no. 12100-1) and IFN-γ (PBL Interferon Source, catalogue no. 12500-2) were used at 500–2,500 U ml^{-1}, and 100–300 ng ml^{-1}, respectively.

A549 transduction and infectivity assays. A549 cells (ATCC catalogue no. CCL-185) were grown in complete media (DMEM (Invitrogen catalogue no. 11965) with 10% FBS (Invitrogen)). A549 stable cell lines were made by gamma-retroviral transduction using either the empty vector control virus (pQXCIP, Clontech), the full-length human *IFITM3* complementary DNA, or a truncated human *IFITM3* cDNA which is missing the first 21 amino acids (NΔ21). After puromycin selection, expression of the IFITM3 and NΔ21 proteins were confirmed by western blotting using an 18% SDS–PAGE gel and an anti-IFITM3 antibody that was raised against the conserved intracellular loop (CIL) of IFITM3 (Proteintech). A549 cell lines were challenged with one of the following strains: A/WSN/33 (a gift of P. Palese), A/California/7/2009, A/Uruguay/716/2007 and B/Brisbane/60/2008 (gift of J. Malbry) for 12 h, then fixed with 4% paraformaldehyde (PFA) and immunostained with anti-HA antibody (Wistar collection) or anti-NP antibodies (Abcam), or Millipore clone H16-L10-4R5 anti-influenza A virus antibody). Per cent infection was calculated from immunofluorescent images as described for the MEF experiments above. Alternatively, cells were transduced with lentiviral vectors to express green fluorescent protein (GFP) or IFITM3 and were stained with anti-NP antibody (Abcam) and analysed by flow cytometry following

challenge with B/Bangladesh/3333/2007 virus (NIMR, England). For the immunofluorescence-based viral titring experiments, virus-containing supernatant was collected from the indicated A549 cell line cultures after 12 h of infection with WSN/33 (part one). Next this supernatant was used to infect MDCK cells (ATCC) in a well by well manner (part two). Both the A549 and MDCK cells were then processed to detect viral HA expression as described above.

LCL infectivity assays. LCL TT and LCL CC cells were grown in RPMI-1640 (Sigma-Aldrich) containing 10% FCS, 2 mM L-glutamine, 1 mM sodium pyruvate, 1× MEM non-essential amino acids solution, and 20 mM HEPES (all from Invitrogen). For infectivity assays, LCL cells were either treated with recombinant human IFN-α2 (PBL Interferon Source, catalogue no. 11100) at 100 units per ml or DPBS (Sigma-Aldrich) for 16 h. The LCL cells were then counted, resuspended at a concentration of 5×10^5 cells per ml, and plated on a 96-well round-bottom plate (200 µl cell suspension per well). The cells were then challenged with WSN/33 influenza A virus (m.o.i. 0.1). After 18 h, the cells were washed twice with 250 µl MACS buffer (DPBS containing 2% FCS and 2 mM EDTA (Sigma-Aldrich)). The cells were fixed and permeabilized using the BD Cytofix/Cytoperm Fixation/Permeabilization Kit (BD Biosciences), following the manufacturer's instructions. Briefly, the cells were resuspended in 100 µl of Cytofix/Cytoperm Fixation and Permeabilization solution and incubated at 4 °C for 20 min. The cells were then washed twice with 250 µl 1× Perm/Wash buffer and resuspended in 50 ml 1× Perm/Wash buffer containing a 2 µg ml^{-1} solution of a fluorescein isothiocyanate (FITC)-conjugated mouse monoclonal antibody against influenza A virus NP (clone 431, Abcam, catalogue no. ab20921). The cells were incubated in the diluted antibody solution for 1 h at 4 °C, washed twice with 250 µl 1× Perm/Wash buffer, resuspended in 200 µl MACS buffer, and analysed by flow cytometry using a BD FACS Calibur (BD Biosciences).

Ethics and sampling. We recruited patients with confirmed seasonal influenza A or B virus or pandemic influenza A pH1N1/09 infection who required hospitalization in England and Scotland between November 2009 and February 2011. Patients with significant risk factors for severe disease and patients whose daily activity was limited by co-morbid illness were excluded. 53 patients, 29 male and 24 female, average age 37 (range 2–62) were selected. 46 (88%) had no concurrent co-morbidities. The remaining 6 had the following comorbid conditions: hypertension (3 patients), alcohol dependency and cerebrovascular disease (1 patient), bipolar disorder (1 patient) and kyphoscoliosis (1 patient). Four patients were pregnant. Where assessed, 36 patients had normal body mass (69%), one had a body mass index <18.5 and 10 had a body mass index between 25 and 39.9 and one a body mass index >40. Seasonal influenza A H3N2, influenza B and pandemic influenza A pH1N1/09 were confirmed locally by viral PCR or serological tests according to regional protocols. Consistent with the prevalent influenza viruses circulating in the UK between 2009 and 2011 (ref. 29) 44 (85%) had pH1N1/09, 2 had pH1N1/09 and influenza B co-infection, 4 had influenza B and 2 had non-subtyped influenza A virus infection. Of the adults, 24 required admission to an intensive care unit (ICU) and 1 required admission to a high dependency unit (HDU). The remainder were managed on medical wards and survived their illnesses. The GenISIS study was approved by the Scotland 'A' Research Ethics Committee (09/MRE00/77) and the MOSAIC study was approved by the NHS National Research Ethics Service, Outer West London REC (09/H0709/52, 09/MRE00/67).

Consent was obtained directly from competent patients, and from relatives/friends/welfare attorneys of incapacitated patients. Anonymized 9-ml EDTA blood samples were transported at ambient temperature. DNA was extracted using a Nucleon Kit (GenProbe) with the BACC3 protocol. DNA samples were re-suspended in 1 ml TE buffer pH 7.5 (10 mM Tris-Cl pH 7.5, 1 mM EDTA pH 8.0).

Sequencing and genetics. Human *IFITM3* sequences were amplified from DNA obtained from peripheral blood by nested PCR (GenBank accession numbers JQ610570 to JQ610621). The first round used primers forward: 5′-TGAGGGT TATGGGAGACGGGGT-3′and reverse: 5′-TGCTCACGGCAGGAGGCC-3′, followed by an additional round using primers forward: 5′-GCTTTGGGGGA ACGGTTGTG-3′and reverse: 5′- TGCTCACGGCAGGAGGCCCGA-3′. The 1.8-kb *IFITM3* band was gel-extracted and purified using the QIAquick Gel Extraction Kit (Qiagen). *IFITM3* was Sanger-sequenced on an Applied Biosystems 3730xl DNA Analyzer (GATC Biotech) using a combination of eight sequencing primers (Supplementary Table 4). Single-nucleotide polymorphisms were identified by assembly to the human *IFITM3* encoding reference sequence (accession number NC_000011.9) using Lasergene (DNAStar). Homozygotes were called based on high, single base peaks with high Phred quality scores, whereas heterozygotes were identified based on low, overlapping peaks of two bases with lower Phred quality scores relative to surrounding base calls (Supplementary Fig. 9). We identified SNP rs12252 in our sequencing and compared the allele and genotype frequencies to allele and genotype frequencies from 1000 Genomes sequencing data from different populations (Supplementary Table 3). In addition, we used the most recent release of phased 1000 Genomes data[30] to impute the region surrounding SNP rs12252 to determine allele frequencies in the publicly available genotype data set of WTCCC1 controls ($n = 2{,}938$) and four previously published data sets genotyped from the Netherlands ($n = 8{,}892$) and Germany ($n = 6{,}253$)[22]. In the imputation, samples genotyped with Illumina 550k, 610k and 670k platforms were imputed against the June 2011 release of 1000 Genotypes phased haplotypes using the Impute software[31], version 2.1.2. Only individuals with European ethnicities (Europe (CEU), Finland (FIN), Great Britain (GBR), Spain/Iberia (IBS), Tuscany (TSI)) were included from the 1000 Genomes reference panel. Recommended settings were used for imputing the region 200 kb in either direction from the variants of interest, along with 1 Mb buffer size. The statistical significance of the allele frequencies was determined by Fisher's exact test.

We assessed for population stratification by principal component analysis. Genotype data from the WTCCC1 1958 Birth Cohort data set were obtained from the European Genotype Archive with permission, reformatted and merged with genotype data from the GenISIS study to match 113,819 SNPs present in both cohorts. Suspected strand mismatches were removed by identifying SNPs with more than 2 genotypes and using the LD method as implemented in Plink (v1.07)[32], resulting in 105,362 matched SNPs. Quality control was applied in GenABEL version 1.6-9 to genotype data for these SNPs for the GenISIS cases and 1,499 individuals from WTCCC. Thresholds for quality control (deviation from Hardy–Weinberg equilibrium ($P < 0.05$), minor allele frequency (MAF) < 0.0005, call rate <98% in all samples) were applied iteratively to identify all markers and subjects passing all quality control criteria, followed by principal component analysis using GenABEL. We tested for positive selection using both a haplotype-based test (|XP-EHH-max|) and allele frequency spectrum-based test statistics, namely the CLR[23–25] on 10-kb windows across the entire genome as described previously[30,33]. The three statistics were combined and the combined *P* value was plotted corresponding to the 10-kb windows.

26. de Wit, E. *et al.* Efficient generation and growth of influenza virus A/PR/8/34 from eight cDNA fragments. *Virus Res.* **103,** 155–161 (2004).
27. Hutchinson, E. C., Curran, M. D., Read, E. K., Gog, J. R. & Digard, P. Mutational analysis of *cis*-acting RNA signals in segment 7 of influenza A virus. *J. Virol.* **82,** 11869–11879 (2008).
28. Britten, K. M., Howarth, P. H. & Roche, W. R. Immunohistochemistry on resin sections: a comparison of resin embedding techniques for small mucosal biopsies. *Biotech. Histochem.* **68,** 271–280 (1993).
29. Ellis, J. *et al.* Virological analysis of fatal influenza cases in the United Kingdom during the early wave of influenza in winter 2010/11. *Eurosurveillance* **16,** 2–7 (2011).
30. The 1000 Genomes project Consortium. A map of human genome variation from population-scale sequencing. *Nature* **467,** 1061–1073 (2010).
31. Howie, B. N., Donnelly, P. & Marchini, J. A flexible and accurate genotype imputation method for the next generation of genome-wide association studies. *PLoS Genet.* **5,** e1000529 (2009).
32. Purcell, S. *et al.* PLINK: a toolset for whole-genome association and population-based linkage analysis. *Am. J. Hum. Genet.* **81,** 559–575 (2007).
33. MacArthur, D. G. *et al.* A systematic survey of loss-of-function variants in human protein-coding genes. *Science* **335,** 823–828 (2012).